Distributed Multi-Object Tracking Under Limited Field of View Sensors

Hoa Van Nguyen, Hamid Rezatofighi, Ba-Ngu Vo, and Damith C. Ranasinghe

Abstract—We consider the challenging problem of tracking multiple objects using a distributed network of sensors. In the practical setting of nodes with limited field of views (FoVs), computing power and communication resources, we develop a *novel distributed multi-object tracking algorithm*. To accomplish this, we first formalise the concept of label consistency, determine a sufficient condition to achieve it and develop a novel *label consensus approach* that reduces label inconsistency caused by objects' movements from one node's limited FoV to another. Second, we develop a distributed multi-object fusion algorithm that fuses local multi-object state estimates instead of local multi-object densities. This algorithm: i) requires significantly less processing time than multi-object density fusion methods; ii) achieves better tracking accuracy by considering Optimal Sub-Pattern Assignment (OSPA) tracking errors over several scans rather than a single scan; iii) is agnostic to local multi-object tracking techniques, and only requires each node to provide a set of estimated tracks. Thus, it is not necessary to assume that the nodes maintain multi-object densities, and hence the fusion outcomes do not modify local multi-object densities. Numerical experiments demonstrate our proposed solution's real-time computational efficiency and accuracy compared to state-of-the-art solutions in challenging scenarios. We also release source code at *https:// github.com/AdelaideAuto-IDLab/Distributed-limitedFoV-MOT* for our fusion method to foster developments in DMOT algorithms.

Index Terms—Multi-sensor multi-object tracking, distributed multi-object tracking, label consistency, track consensus.

I. INTRODUCTION

THe aim of Multi-Object Tracking (MOT) is to estimate an unknown and time-varying number of object trajectories from noisy sensor measurements. MOT is an integral component in a multitude of applications in diverse domains, including surveillance [1], robotics [2]–[4], computer vision [5], traffic monitoring [6], [7], cell biology [8], [9], and space exploration [10]. However, MOT is complicated by a time-varying number of objects, false alarms, misdetections, and data association uncertainty, in addition to the uncertainty resulting from process and measurement noise [11]. There are three notable frameworks, amongst a range of algorithms,

for tackling an MOT problem: multiple hypotheses tracking (MHT) [12], joint probabilistic data association (JPDA) [1], and random finite set (RFS) [11].

Recently, driven by progress in wireless communication and sensing technologies, sensor networks comprising of interconnected *nodes or agents* with sensing, communication and processing capabilities have attracted considerable research interest [13]–[15]. Importantly, for MOT, a network of multiple sensing nodes addresses the practical and critical problem of limited observability of sensing modalities at a single node, especially where objects are distributed across large spatial regions [10], for example, tracking space debris using a network of low-earth-orbit cube satellites [16]. Sensor networks enable the inference of more accurate trajectories by *fusing information* (*e.g.*, estimates or densities) of multi-objects from observations at individual nodes (with limited observability) in a scalable (with respect to the number of nodes), flexible and reliable (*i.e.*, resilient to failures) manner [17]. However, leveraging these benefits requires a *distributed mode* of operation for MOT where each node operates independently, without any knowledge of the network topology. Consequently, due to the significant benefits possible from using sensor networks for multi-object tracking applications, distributed MOT (DMOT) has attracted researchers' growing interest in recent years.

DMOT is a nontrivial problem and entails additional challenges. In particular, a suitable fusion algorithm is required to combine *common information* associated with multi-objects to achieve improved tracking accuracy whilst merging *complementary information* to overcome the limited FoV of a single sensor node. In principle, optimal fusion can be achieved by preserving marginal and joint multi-object distributions from all nodes [18]. However, maintaining these distributions requires sharing common information among all nodes [13], [19], which limits the flexibility and scalability of the network. To maintain flexibility and scalability, robust (but sup-optimal) fusion solutions have been developed to address the double-counting of information when the common information is unknown [20].

Recent fusion techniques for DMOT were mostly developed from the random finite set framework because it facilitates principled generalisation of (single-object) distributed estimation to the multi-object case [19]. This framework offers a convenient notion of multi-object (probability) density that enabled the development of a suite of multi-object filters, *e.g.*, the probability hypothesis density (PHD) [21], cardinalised PHD (CPHD) [22], multi-Bernoulli (MB) [11], [23], [24], and labelled multi-Bernoulli (LMB) [25], generalised labelled multi-Bernoulli (GLMB) [26], [27], and multi-scan

GLMB [28] filters. Many of these filters have been adapted for distributed multi-object estimation via the concept of Generalised Covariance Intersection (GCI[1]) [19], [34], *e.g.*, PHD-GCI [20], CPHD-GCI [13], MB-GCI [35], LMB-GCI [36], and its variations [15], [37], [38].

When the nodes do not *share the same Field of View (FoV)*, which is invariably the case with distributed sensor networks, GCI-based filters tend to perform poorly [39]. A remedy for the PHD-GCI filter was proposed using cluster analysis (CA-PHD-GCI) [40]. However, this approach requires sharing FoV information among nodes and does not generate *object labels (identities)*, an important function of an MOT algorithm [1]. Labelled GCI-based filters generate object labels but tend to suffer from label inconsistency (*i.e.*, individual objects are assigned different labels by different nodes). While there are efforts to reduce label inconsistency for sensors *without FoV limitations* [15], [37], [38], the *more practical problems of reaching label consensus and reducing label inconsistency in distributed fusion with limited FoV sensors have not been addressed*. In addition to GCI, which is based on log-linear geometric averaging of probability densities, the linear arithmetic average has also been explored in the PHD [41]–[44], CPHD [45], and MB filter [46]. However, the arithmetic averaging consensus for DMOT has not yet been developed.

While current fusion algorithms based on multi-object densities offer elegant conceptual solutions, these methods require intensive computing resources and high communication bandwidth. Due to the combinatorial nature of MOT, each multi-object distribution is characterised by a huge number of parameters. The computing resources needed to calculate these parameters at the nodes and the bandwidth needed for communicating them to neighbouring nodes can be prohibitive for real-time DMOT with increasing numbers of networked nodes and objects [47]. The high computational time and bandwidth requirements can be circumvented by considering the distributed fusion of local multi-object state estimates instead of multi-object densities. The track-to-track fusion and association algorithms investigated in [48]–[55] assume no false tracks nor missed objects, *i.e.*, the number of local tracks from any two nodes are the same [54]. This assumption is not practical in problems involving a time-varying number of objects and/or networks with limited FoV sensors. Further, most of the discussed distributed fusion approaches require *feedback* [56], *i.e.*, the fusion outcome is used to update the local multi-object densities.

In this work, we propose an efficient distributed fusion algorithm for DMOT that accounts for practical limitations on computing and communication resources as well as sensors with different and limited FoVs *without feedback (i.e., the local multi-object densities are not modified)*. Our solution fuses local multi-object state estimates, and thus, is agnostic to local multi-object tracking techniques. It employs a *novel label consensus* algorithm that reduces inconsistency in the estimated labels caused by objects moving from one node's

---

[1]GCI is also known as Chernoff fusion [29], [30], Exponential Mixture Density [20], [31], [32] or Kullback-Leibler Average [13], [14], [33]
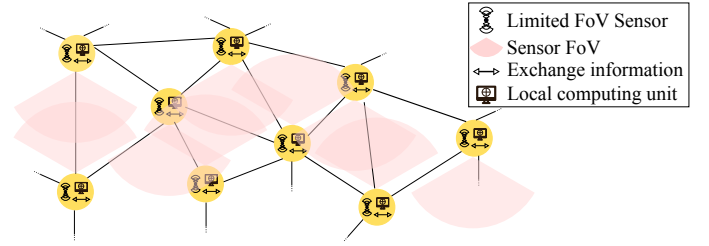

Fig. 1. A distributed sensor network system with limited FoVs.

limited FoV to another. The optimal solution to this problem is NP-hard (for more than 2 nodes). Considering the real-time requirements in practical applications, we propose a tractable sub-optimal fusion solution that reduces label inconsistency. This strategy incurs far less computation time and bandwidth than multi-object filtering density-based solutions. It also achieves better tracking accuracy by considering the tracking errors over several scans using the Optimal Sub-Pattern Assignment (OSPA) metric with OSPA track-to-track distance or OSPA$^{(2)}$ metric [57]–[59]. We also formalise the label consistency concept and derive a sufficient condition to achieve label consistency by exploiting the metric properties of the OSPA$^{(2)}$. To validate our proposed method's effectiveness, we benchmark its accuracy and fusing time against state-of-the-art GCI-based solutions for MOT in a series of numerical experiments.

The paper is organised as follows. We define the problem and provide background on metrics in Section II. Section III presents our proposed fusion method. Section IV details numerical experiments, results and comparisons with GCI-based methods. Section V discusses concluding remarks.

II. BACKGROUND

This section provides the necessary background on distributed sensor networks and multi-object error metrics.

A. Distributed sensor network description

Fig. 1 depicts a distributed heterogeneous network described by an undirected graph $G = (\mathcal{N}, \mathcal{A})$, where $\mathcal{N}$ is the set of nodes and $\mathcal{A} \in \mathcal{N} \times \mathcal{N}$ is the set of arcs representing connections among nodes. An arc $(a, b) \in \mathcal{A}$ means that node a can receive data from node b and vice-versa. We denote by $\mathcal{N}^{(a)} \triangleq \{b \in \mathcal{N} : b \neq a \text{ and } (a, b) \in \mathcal{A}\}$ the set of neighbours of node a from which data can be obtained. Each node is typically assigned with a unique ID. The set of all such IDs forms an ordered set (*e.g.*, integers), and is assumed to be known by all the nodes.

Consider the task of monitoring a large area using the network of Fig. 1 to detect and track an unknown and time-varying number of mobile objects. We assume that each node is equipped with a local computing unit capable of computing local multi-object state estimates, as well as a transceiver for communicating reliably with their neighbours through a limited range-and-bandwidth communication channel. In this context, each node can communicate its local multi-object state estimates to other nodes directly or indirectly using a typical

TABLE I
LIST OF VARIABLES/PARAMETERS

| Symbol	Variable/Parameter
$\mathcal{N}$	set of nodes
$\mathcal{A}$	set of arcs among nodes
$\mathcal{N}^{(a)}$	set of neighbours of nodes a
$\mathbb{X}$	single-object state space
$\mathbb{L}$	label space
$\mathbb{T}$	track space
$\mathbb{K}$	discrete-time space
$\mathbb{I} = \mathbb{L} \times \mathcal{N}$	global label space
$\mathbf{x} = (x, \ell)$	labelled state
$\mathbf{X} \subset \mathbb{X} \times \mathbb{L}$	labelled multi-object state
$\mathcal{L}(\mathbf{X}) \subset \mathbb{L}$	set of labels of $\mathbf{X}$
$\mathbf{t} = (t, \ell)$	labelled track
$\bar{\mathbf{t}}$	labelled track estimate after fusion
$\mathcal{D}^{(\mathbf{t})} \subseteq \mathbb{K}$	set of time instances that $\mathbf{t}$ exists
$\mathbf{T} \subset \mathbb{T} \times \mathbb{L}$	set of labelled tracks
$\mathcal{T}(\mathbf{T}) \subset \mathbb{T}$	set of unlabelled tracks of $\mathbf{T}$
$\mathbf{X}^{(a)} \subset \mathbb{X} \times \mathbb{I}$	set of globally labelled state estimates of node a
$\mathbf{L}^{(a)} \subset \mathbb{I}$	set of global labels of node a
$\mathbf{T}^{(a)} \subset \mathbb{T} \times \mathbb{I}$	set of globally labelled tracks of node a
$\mathbf{X}^{(con)} \subset \mathbb{X} \times \mathbb{I}$	set of consensed globally labelled state estimates

ad-hoc network or mesh network, for example, using an IEEE 802.16 standard. Each node is equipped with a limited field-of-view (FoV) sensor subjected to false alarms and misdetections. The network of interest has no central fusion node, and its nodes operate without knowledge of the network topology.

At time k, an existing object is represented by a *labelled state* $\mathbf{x}_k = (x_k, \ell_k)$, where $x_k \in \mathbb{X}$ is its *state* vector, and $\ell_k \in \mathbb{L}$ is a unique label consisting of the time of birth and an index to distinguish objects born at the same time. The set $\mathbf{X}_k \subset \mathbb{X} \times \mathbb{L}$ of labelled states of existing objects (with distinct labels) is called the *labelled multi-object state* (the set $X_k \subset \mathbb{X}$ of states of existing objects is called the *multi-object state*). We use the notation $|X|$ for the cardinality of a set X, and $\mathcal{L}(\mathbf{X}) = \{\mathcal{L}(\mathbf{x}) : \mathbf{x} \in \mathbf{X}\}$ for the set of labels of a multi-object state $\mathbf{X}$, where $\mathcal{L} : \mathbb{X} \times \mathbb{L} \to \mathbb{L}$ is the label projection defined by $\mathcal{L}((x, \ell)) = \ell$.

Definition 1. Given a (discrete) time window $\mathbb{K} \triangleq \{1, \ldots, K\}$ from start time 1 to end time K of the scenario, the *track space* $\mathbb{T}$ is the space of all functions $t : \mathbb{K} \to \mathbb{X}$. Any element $t \in \mathbb{T}$ is called a *track*, and the ordered pair $\mathbf{t} = (t, \ell) \in \mathbb{T} \times \mathbb{L}$ is called a *labelled track*.

The set $\mathcal{D}^{(\mathbf{t})} \subseteq \mathbb{K}$ of time instances that the track $\mathbf{t} = (t, \ell)$ exists is the domain $\mathcal{D}^{(t)}$ of t, and the labelled state vector at time $k \in \mathcal{D}^{(\mathbf{t})}$ is given by $\mathbf{x}_k = (t(k), \ell)$. We also use the same notation for the label projection $\mathcal{L}((t, \ell)) = \ell$, and $\mathcal{L}(\mathbf{T}) = \{\mathcal{L}(\mathbf{t}) : \mathbf{t} \in \mathbf{T}\}$, for $\mathbf{T} \subset \mathbb{T} \times \mathbb{L}$. Further, let $\mathcal{T} : \mathbb{T} \times \mathbb{L} \to \mathbb{T}$ be the track projection defined by $\mathcal{T}((t, \ell)) = t$ and $\mathcal{T}(\mathbf{T}) = \{\mathcal{T}(\mathbf{t}) : \mathbf{t} \in \mathbf{T}\}$.

Two remarks are in order. First, the definition of labelled tracks meets the MOT requirement that tracks have *labels (or identities)* [1]. In practice, labels are important for identifying/referencing tracks; for example, given multiple tracks on display, it would be impractical for a human user to
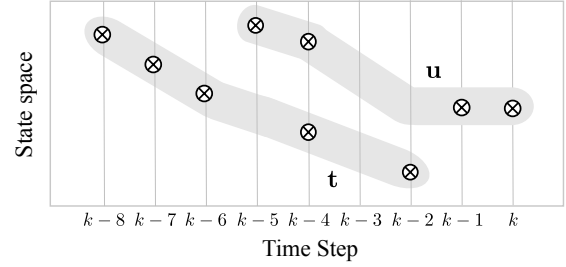
Fig. 2. A set of two fragmented tracks $\mathbf{t}$ and $\mathbf{u}$.

communicate with other users about a track by specifying every estimated position of its trajectory. Second, the set $\mathcal{D}^{(\mathbf{t})}$ of instances that track $\mathbf{t}$ exists need not be consecutive (see Fig. 2), and hence encompasses the so-called *fragmented tracks* generated by many MOT algorithms. A *fragmented track* arises when the MOT algorithm declares it non-existent (possibly due to misdetections) in between instances where it (is declared to) exist, as illustrated in Fig. 2. When $\mathcal{D}^{(\mathbf{t})}$ consists of consecutive instances, track $\mathbf{t}$ is called a *trajectory*.

Given a finite set $\mathbf{T} \subset \mathbb{T} \times \mathbb{L}$ of labelled tracks with distinct labels, the labelled multi-object state at time $k \in \mathbb{K}$ is given by $\mathbf{X}_k = \cup_{(t,\ell) \in \mathbf{T}} \{(t(k), \ell)\}$. Note that the history $\mathbf{X}_{1:K} \triangleq \mathbf{X}_1, \ldots, \mathbf{X}_K$ of labelled multi-object states completely determines the set $\mathbf{T}$, and hence we use the notation $\mathbf{X}_{1:K}$ to denote the set of labelled tracks on the interval $\mathbb{K}$. We denote the restriction of the track t, labelled track $\mathbf{t}$, and set of labelled tracks $\mathbf{X}_{1:K}$ (or $\mathbf{T}$) on the window $\{j : k\} \subset \mathbb{K}$, by $t_{j:k}$, $\mathbf{t}_{j:k}$, and $\mathbf{X}_{j:k}$ (or $\mathbf{T}_{j:k}$). Hereon, the discussions in this paper only concern the time window $\{j : k\}$, hence, for notational compactness, we drop the subscript $j : k$ when no confusion arises, *e.g.*, $\mathbf{T} \triangleq \mathbf{T}_{j:k}$.

Instead of seeking consensus amongst local multi-object densities as pursued in many of the latest works [15], [40], we are interested in reaching consensus amongst local multi-object state estimates from the set $\mathcal{N}$ of nodes. At time k, each local node a communicates a message which is an ordered pair $(a, \mathbf{X}_k)$ comprising of the node's identity a and the local labelled multi-object state estimate $\mathbf{X}_k$. Let $\mathbb{I} = \mathbb{L} \times \mathcal{N}$ be the global label space of the network, wherein each global label is unique across the network. Let $\mathbf{X}_k^{(a)} = \{(x, (\ell, a)) : (x, \ell) \in \mathbf{X}_k\} \subset \mathbb{X} \times \mathbb{I}$ be the globally labelled multi-object state estimate of node a at time k generated from the communicated message $(a, \mathbf{X}_k)$, and $\mathbf{L}_k^{(a)} = \mathcal{L}(\mathbf{X}_k^{(a)}) = \{\boldsymbol{\ell} \triangleq (\ell, a) : \ell \in \mathcal{L}(\mathbf{X}_k)\} \subset \mathbb{I}$ be its corresponding set of global labels. The receiving node (*e.g.*, $b \in \mathcal{N}^{(a)}$) stores $\mathbf{X}_k^{(a)}$ in its own memory to form a set of globally labelled tracks $\mathbf{X}^{(a)}$ (or $\mathbf{T}^{(a)} \subset \mathbb{T} \times \mathbb{I}$) from node a. Given the sets of globally labelled track estimates $\{\mathbf{T}^{(a)}\}_{a \in \mathcal{N}}$, our objective is to compute a consensed globally labelled multi-object state estimate $\mathbf{X}_k^{con} \subset \mathbb{X} \times \mathbb{I}$ by reaching a consensus on the latest labelled multi-object state estimates $\{\mathbf{X}_k^{(a)}\}_{a \in \mathcal{N}}$ in terms of kinematics and labels. Moreover, we seek an efficient algorithm that is scalable with respect to (wrt) network size. A list of symbols is provided in Table I.

Our solution is based on minimising the overall dissimilarity of tracks between sensor nodes. We employ a metric to

measure such dissimilarities. Thus, in the next subsection, we revisit the metric property and a widely used metric in evaluating the tracking performance of MOT algorithms.

B. Multi-object metrics

A function $d : \mathcal{S} \times \mathcal{S} \rightarrow [0, \infty)$ is called a *metric* or a *distance* function on the space $\mathcal{S}$ if it meets the following conditions:

1) $d(x, y) = 0$ if and only if $x = y$ (identity),
2) $d(x, y) = d(y, x)$ (symmetry),
3) $d(x, y) \leq d(x, z) + d(z, y)$ (triangle inequality).

We are interested in distances between two finite subsets $X = \{x^{(1)}, \ldots, x^{(m)}\}$ and $Y = \{y^{(1)}, \ldots, y^{(n)}\}$ of a space equipped with a metric d, referred to as the base-distance (between the elements of X and Y). An example of particular relevance to this work is the Optimal Sub-Pattern Assignment (OSPA) metric.

Let $d^{(c)}(x, y) \triangleq \min(c, d(x, y))$, and Π_n be the set of all permutations of $\{1, 2, ..., n\}$. The *OSPA* metric of (integer) order $p \geq 1$ and cut-off $c \in (0, \infty)$ is defined as [60]:

$$d_0^{(p,c)}(X, Y) \tag{1}$$
$$= \left(\frac{1}{n} \left(\min_{\pi \in \Pi_n} \sum_{i=1}^{m} d^{(c)}(x^{(i)}, y^{(\pi(i))})^p + c^p(n - m) \right) \right)^{1/p},$$

if $m \leq n$, and $d_0^{(p,c)}(X, Y) \triangleq d_0^{(p,c)}(Y, X)$, if $m > n$, in addition, $d_0^{(p,c)}(X, Y) = c$ if one of the argument is empty, and $d_0^{(p,c)}(\emptyset, \emptyset) = 0$. The two adjustable parameters p, and c, are interpreted as the outlier and cardinality sensitivities, respectively. The OSPA metric can be interpreted as the best-case localisation and cardinality error per object.

Given a meaningful base-distance $d^{(c)}(\cdot, \cdot)$ between two tracks, the OSPA metric provides meaningful distances between two finite subsets of tracks. One such base distance is the time-averaged OSPA distance between the states of two tracks over time instances when at least one of the tracks exists [59]. Specifically, for any $t, u \in \mathbb{T}$, the *OSPA track-to-track distance* is defined as

$$\tilde{d}^{(c)}(t, u) = \sum_{k \in \mathcal{D}^{(t)} \cup \mathcal{D}^{(u)}} \frac{d_0^{(c)}(\{t(k)\}, \{u(k)\})}{|\mathcal{D}^{(t)} \cup \mathcal{D}^{(u)}|} \tag{2}$$

if $\mathcal{D}^{(t)} \cup \mathcal{D}^{(u)} \neq \emptyset$, and $\tilde{d}^{(c)}(t, u) = 0$, if $\mathcal{D}^{(t)} \cup \mathcal{D}^{(u)} = \emptyset$, where $d_0^{(c)}(\{t(k)\}, \{u(k)\})$ denotes the OSPA distance, and since the arguments are only sets of at most one element, the parameter p no longer comes into play. For example, the OSPA track-to-track distance between the tracks $\mathbf{t}$ and $\mathbf{u}$ in Fig. 2 is

$$\tilde{d}^{(c)}(t, u) = \left(7c + d_0^{(c)}(\{t(k-4)\}, \{u(k-4)\}) \right)/8.$$

The OSPA metric with OSPA track-to-track distance in (2), called OSPA-on-OSPA or OSPA$^{(2)}$, provides a natural distance between two sets of tracks. This distance can be interpreted as the time-averaged per-track error and demonstrates meaningful behaviour on various MOT scenarios. Errors in localisation, cardinality, track fragmentation and track identity switching

all yield intended increases in the OSPA$^{(2)}$ error. The higher the frequency of track fragmentation and identity switches, the higher the OSPA$^{(2)}$ error. A dropped track that later regained with the same identity yields a smaller increase in OSPA$^{(2)}$ error than if it were regained with a different identity [59].

III. FUSION USING TRACK CONSENSUS

This section presents a novel algorithm for fusing the latest local labelled multi-object state estimates among the distributed network of sensor nodes. Our innovation is based on the dissimilarity of tracks between nodes over multiple scans (*i.e.*, time window) instead of relying on the multi-object densities at a single scan as in previous works. Fusing multi-object state estimates instead of multi-object densities significantly reduces the processing time and bandwidth. Moreover, the proposed solution applies to non-overlapping or partially overlapping limited FoVs of sensor nodes and improves tracking accuracy and cardinality estimations (or *detectability* of objects).

We first consider the problem of measuring the dissimilarity between tracks. For this purpose, we define optimal track matching via the OSPA track-to-track distance. Based on the notion of optimal track matching, we formalise the concept of label consistency and derive a sufficient condition to achieve it. We then develop a novel algorithm for *track consensus* by *i)* formulating a method for achieving kinematic consensus between track estimates made by two nodes (Section III-C); *ii)* extending this to a pair-wise fusion algorithm for kinematic consensus when the number of nodes is greater than two (Section III-D); and *iii)* developing a label consensus algorithm to achieve label consistency across the distributed network of nodes (Section III-E).

A. Optimal track matching

Consider two nodes $a, b \in \mathcal{N}$. Without loss of generality, suppose that fusion is performed at node a. At time k, the aim is to compute a consensed labelled multi-object state estimate $\mathbf{X}_k^{(a,\mathrm{con})}$ at node a from $\mathbf{X}_k^{(a)}$ and $\mathbf{X}_k^{(b)}$. Since $\mathbf{X}_k^{(a,\mathrm{con})}$ is computed from the latest local labelled multi-object state estimates, previously terminated tracks have no influence, only tracks declared to *exist* at k are considered. With a slight abuse of notation, let $\mathbf{T}_k^{(a)} = \{\mathbf{t} \in \mathbf{T}^{(a)} : \mathcal{L}(\mathbf{t}) \in \mathcal{L}(\mathbf{X}_k^{(a)})\}$ be the set of live tracks at k, as declared by node a, truncated on the window $[j : k]$, and likewise for $\mathbf{T}_k^{(b)} = \{\mathbf{t} \in \mathbf{T}^{(b)} : \mathcal{L}(\mathbf{t}) \in \mathcal{L}(\mathbf{X}_k^{(b)})\}$. For notational compactness, we use the shorthand $a^{(m)} = \mathcal{T}(\mathbf{a}^{(m)}), b^{(m)} = \mathcal{T}(\mathbf{b}^{(m)})$, and $u^{(m)} = \mathcal{T}(\mathbf{u}^{(m)})$.

Definition 2. Given two sets of tracks $\mathbf{T}_k^{(a)} = \{\mathbf{a}^{(1)}, \ldots, \mathbf{a}^{(|\mathbf{T}_k^{(a)}|)}\}$ and $\mathbf{T}_k^{(b)} = \{\mathbf{b}^{(1)}, \ldots, \mathbf{b}^{(|\mathbf{T}_k^{(b)}|)}\}$, assuming that $|\mathbf{T}_k^{(a)}| \leq |\mathbf{T}_k^{(b)}|$. We define the optimal matching as the pairing of elements between the two sets that yields the OSPA$^{(2)}$ distance $d_0^{(1,c)}(\mathcal{T}(\mathbf{T}_k^{(a)}), \mathcal{T}(\mathbf{T}_k^{(b)}))$ *i.e.*,

$$\pi^* = \arg\min_{\pi \in \Pi_{|\mathbf{T}_k^{(b)}|}} \sum_{m=1}^{|\mathbf{T}_k^{(a)}|} \tilde{d}^{(c)}(a^{(m)}, b^{(\pi(m))}), \tag{3}$$

Here, $\pi^*(m) = n$ means track $\mathbf{a}^{(m)} \in \mathbf{T}_k^{(a)}$ is matched to track $\mathbf{b}^{(n)} \in \mathbf{T}_k^{(b)}$.

The optimal assignment problem can be solved using the Hungarian algorithm [61], [62] with $\mathcal{O}(|\mathbf{T}_k^{(b)}|^4)$ complexity, or using efficient algorithms in [63]–[65] with $\mathcal{O}(|\mathbf{T}_k^{(b)}|^3)$ complexity.

Remark 1. The processing time of computing the optimal assignment in (3) is considerably shorter than that of LM-GCI in [15] where each node runs an LMB filter. The reason is that for the LMB filter, the multi-object state estimate is extracted from the LMB density for any label with existence probabilities higher than a predefined threshold (typically 0.5). Thus, the number of tracks used in (3) is substantially smaller than the number of LMB components used in LM-GCI. Additionally, for optimal matching, we need to compute the distance between two tracks (for our method) or two LMB components (for LM-GCI). The computational complexity of computing OSPA$^{(2)}$ distance between two tracks is considerably smaller than the computing distance (GCI-divergence) between two LMB components wherein a Gaussian mixture characterises the spatial density of each component.

B. Label consistency and performance bound

In this subsection, we formalise the concept of label consistency for the consensus of labelled tracks. Note that while the term label consistency/inconsistency has been used in the context of DMOT in [37], there is no formal definition.

Definition 3. *Let* $\mathbf{u}^{(1)}, \ldots, \mathbf{u}^{(N)} \in \mathbb{T} \times \mathbb{I}$ *be the true trajectories of N distinct objects. Let* $\mathbf{a}^{(1)}, \ldots, \mathbf{a}^{(N)}$ *be their corresponding track estimates at node a, and* $\mathbf{b}^{(1)}, \ldots, \mathbf{b}^{(N)}$ *be their corresponding track estimates at node b. Then, we say that label consistency is achievable when the optimal matching π^* between these sets of track estimates satisfies*

$$\pi^*(m) = m, \ \forall m \in \{1, \ldots, N\}. \tag{4}$$

Moreover, suppose that for each $m \in \{1, \ldots, N\}$ the tracks $\mathbf{a}^{(m)}$ and $\mathbf{b}^{(m)}$ are assigned new labels, resulting in tracks $\bar{\mathbf{a}}^{(m)}$ and $\bar{\mathbf{b}}^{(m)}$. Then, we say label consistency is achieved if

$$\mathcal{L}(\bar{\mathbf{a}}^{(m)}) = \mathcal{L}(\bar{\mathbf{b}}^{(m)}), \ \forall m \in \{1, \ldots, N\}. \tag{5}$$

In essence, label consistency is achieved if the same object is assigned the same global label by two nodes. Otherwise, we have label inconsistency.

Remark 2. Definition 3 can be easily extended to more than two nodes. Suppose that $\bar{\mathbf{t}}^{(1)}, \ldots, \bar{\mathbf{t}}^{(|\mathcal{N}|)} \in \mathbb{T} \times \mathbb{I}$ are the globally labelled track estimates of a true trajectory $\mathbf{u}$. Then label consistency is achieved if

$$\mathcal{L}(\bar{\mathbf{t}}^{(m)}) = \mathcal{L}(\bar{\mathbf{t}}^{(n)}), \ \forall m, n \in \{1, \ldots, |\mathcal{N}|\}. \tag{6}$$

The following result provides the conditions to achieve label consistency (see Appendix A for proofs).

Proposition 1. Consider the trajectories $\mathbf{u}^{(1)}, \ldots, \mathbf{u}^{(N)}$ of $N \leq \min(|\mathbf{T}_k^{(a)}|, |\mathbf{T}_k^{(b)}|)$ distinct objects where $\mathbf{T}_k^{(a)}$ and $\mathbf{T}_k^{(b)}$ are the sets of live tracks at time k at node a and

node b, respectively. Let us denote their corresponding labelled track estimates at nodes a and b, by $\mathbf{a}^{(1)}, \ldots, \mathbf{a}^{(N)}$ and $\mathbf{b}^{(1)}, \ldots, \mathbf{b}^{(N)}$. Suppose that their track-to-track errors $\tilde{d}^{(c)}(a^{(m)}, u^{(m)})$, $\tilde{d}^{(c)}(u^{(m)}, b^{(m)})$ at nodes a and b, are bounded by $\mathcal{E}$ for all $m \in \{1, \ldots, N\}$, and that:

$$\tilde{d}^{(c)}(a^{(m)}, b^{(n)}) = c \ \forall m > N, \forall n \in \{1, \ldots, |\mathbf{T}_k^{(b)}|\},$$
$$\tilde{d}^{(c)}(a^{(m)}, b^{(n)}) = c \ \forall m \in \{1, \ldots, |\mathbf{T}_k^{(a)}|\}, \forall n > N. \tag{7}$$

Then, to achieve label consistency for these N distinct objects, we need

$$\tilde{d}^{(c)}(u^{(m)}, u^{(n)}) > 4\mathcal{E} \ \forall m, n \in \{1, \ldots, N\}, m \neq n. \tag{8}$$

For a given upper bound on the track-to-track error, the above result provides a lower bound on the separation of the true trajectories required to achieve label consistency. A conservative track-to-track error bound can be determined from the kinematic error and the frequency of misses or the empirical existence probability.

Definition 4. The empirical existence probability of a track t over the time interval $\{j : k\}$ is defined as

$$P_X(t) = \frac{|\mathcal{D}^{(t)}|}{k - j + 1}, \tag{9}$$

where $\mathcal{D}^{(t)} \subseteq \{j : k\}$ is the domain of track t.

Proposition 2. Let $P_X^{\min}$ be minimum empirical existence probabilities of all tracks at nodes a and b, *i.e.*,

$$P_X^{\min} = \min_{\mathbf{t} \in \mathbf{T}_k^{(a)} \cup \mathbf{T}_k^{(b)}} P_X(\mathcal{T}(\mathbf{t})), \tag{10}$$

Suppose the single-scan estimation errors at nodes a and b are bounded as follows:

$$d_0^{(c)}(\{a^{(m)}(i)\}, \{u^{(m)}(i)\}) = \begin{cases} c & i \notin \mathcal{D}^{(\mathbf{a}^{(m)})} \\ d^{(c)}(a^{(m)}(i), u^{(m)}(i)) \leq \varepsilon & i \in \mathcal{D}^{(\mathbf{a}^{(m)})} \end{cases},$$
$$d_0^{(c)}(\{b^{(m)}(i)\}, \{u^{(m)}(i)\}) = \begin{cases} c & i \notin \mathcal{D}^{(\mathbf{b}^{(m)})} \\ d^{(c)}(b^{(m)}(i), u^{(m)}(i)) \leq \varepsilon & i \in \mathcal{D}^{(\mathbf{b}^{(m)})} \end{cases},$$
$$\forall m \in \{1, \ldots, N\}.$$

Then the track-to-track error is bounded by

$$\varepsilon P_X^{\min} + c(1 - P_X^{\min}). \tag{11}$$

Remark 3. If the window $[j : k]$ is long enough, and a "good" multi-object tracker (*e.g.*, MHT [12], GLMB [26], [27] or multi-scan GLMB [28]) is used, then it is possible to have $P_X^{\min} \geq P_D$ where P_D is the detection probability. Thus:

$$\varepsilon P_X^{\min} + c(1 - P_X^{\min}) \leq \varepsilon P_D + c(1 - P_D), \tag{12}$$

and the condition for label consistency is

$$\tilde{d}^{(c)}(u^{(m)}, u^{(n)}) > 4\big[\varepsilon P_D + c(1 - P_D)\big],$$
$$\forall m, n \in \{1, \ldots, N\}, m \neq n. \tag{13}$$

Intuitively, (13) suggests that to achieve label consistency it is necessary that *i)* the object true trajectories are reasonably well-separated; *ii)* the detection probability P_D is relatively high.

C. Kinematic consensus for two nodes

Track consensus involves kinematic consensus and label consensus. In this subsection, we develop an algorithm to compute the *kinematic consensus* between track estimates from two nodes. This kinematic consensus algorithm is extended to multiple nodes in Section III-D, while the label consensus algorithm is discussed in Section III-E.

Since each node is equipped with a limited FoV sensor, only track estimates within the overlapped FoV of two sensors (observed[2] by both nodes' FoVs) should be matched and fused to enhance tracking accuracy. Further, the unmatched tracks (outside the overlapped FoV of two sensors) should be retained to improve detectability. Thus, the set of tracks at each node can be divided into three subsets: *i)* matched tracks, *ii)* unmatched and retained tracks, *iii)* unmatched and discarded tracks. However, for distributed sensor networks, the sensor FoV information of other nodes is usually unknown, and we rely on the separation between two-track estimates to determine if they are matched or not. For all pairs (m, n) such that $\pi^*(m) = n$, only pairs with associated costs $C_{m,n} = \tilde{d}^{(c)}(a^{(m)}, b^{(n)})$ less than c are considered matched. Essentially, this implies that both matched tracks must exist together for at least one instance (*e.g.*, at time $k - 4$ as in Fig. 2) or are not too distant in accordance with the cut-off distance c.

$$
\begin{aligned}
m &\in Q_k^{(a)} \subseteq \{1, \ldots, |\mathbf{T}_k^{(a)}|\}, \\
n &\in Q_k^{(b)} \subseteq \{1, \ldots, |\mathbf{T}_k^{(b)}|\}, \\
&\text{subject to } \pi^*(m) = n, C_{m,n} < c.
\end{aligned}
\tag{14}
$$

The steps for determining matched pairs are given in Algorithm B.1 (see Appendix B).

For the unmatched tracks, some of these can be false tracks and should be discarded. Thus, we propose that only unmatched tracks with lengths higher than a predefined track length $\mathcal{C}_{\text{len}}$ are retained. Similar to the traditional thresholding method in extracting raw measurements, a small track length $\mathcal{C}_{\text{len}}$ helps to initiate new objects faster albeit with more false-positives and vice versa [66]. Intuitively, $\mathcal{C}_{\text{len}}$ delays the confirmation of a new object by the track consensus algorithm for at least $\mathcal{C}_{\text{len}}$ steps, *i.e.*, the observed track must have a track length greater than or equal to $\mathcal{C}_{\text{len}}$ to be confirmed as a new birth object. As a result, the consensed labelled multi-object state estimate comprises of two components: *i)* the matched and fused labelled state estimates, *ii)* the unmatched and retained labelled state estimates of two nodes. The steps for fusing two nodes are described in Algorithm 1, and elaborated on below:

Step 1) Fuse matched labelled state estimates: We compute[3] the set $\bar{\mathbf{X}}_k^{(a)}$ of matched labelled state estimates at node a by

---

Algorithm 1 FuseTwoNodes

Input: $\mathbf{T}_k^{(a)}$; $\mathbf{T}_k^{(b)}$; $\Xi_{1:k-1}^{(a,b)}$; $\mathbf{L}_{1:k-1}^{(a)}$; $\mathbf{L}_{1:k-1}^{(b)}$; $\mathcal{C}_{\text{len}}$;
Output: $\mathbf{X}_k^{(a,\text{con})}$; $\Xi_{1:k}^{(a,b)}$; $\mathbf{L}_{1:k}^{(a)}$; $\mathbf{L}_{1:k}^{(b)}$;
1: $\mathbf{L}_{1:k}^{(a)} = \mathbf{L}_{1:k-1}^{(a)} \cup (\mathcal{L}(\mathbf{T}_k^{(a)}) \setminus \mathbf{L}_{1:k-1}^{(a)})$;
2: $\mathbf{L}_{1:k}^{(b)} = \mathbf{L}_{1:k-1}^{(b)} \cup (\mathcal{L}(\mathbf{T}_k^{(b)}) \setminus \mathbf{L}_{1:k-1}^{(b)})$;
3: $Q_k := \text{DetermineMatchedPairs}(\mathbf{T}_k^{(a)}, \mathbf{T}_k^{(b)})$;
4: $\Xi_{1:k}^{(a,b)} := \text{UpdateMatchedHistory}(\Xi_{1:k-1}^{(a,b)}, \mathbf{L}_{1:k}^{(a)}, \mathbf{L}_{1:k}^{(b)}, Q_k)$;
5: Compute $\bar{\mathbf{X}}_k^{(a)}$ via (15) ; $\mathbf{X}_k^{(a,\text{ret})}$ and $\mathbf{X}_k^{(b,\text{ret})}$ via (16) ;
6: $\mathbf{X}_k^{(a,\text{con})} := \bar{\mathbf{X}}_k^{(a)} \cup \mathbf{X}_k^{(a,\text{ret})} \cup \mathbf{X}_k^{(b,\text{ret})}$;

---

fusing matched labelled state estimates, *i.e.*,

$$
\bar{\mathbf{X}}_k^{(a)} = \{(x, \boldsymbol{\ell}^{(m)}) : x = w^{(a)}a^{(m)}(k) + w^{(b)}b^{(n)}(k), (m, n) \in Q_k\},
\tag{15}
$$

where $w^{(a)}$ and $w^{(b)}$ be the fusing weights of two nodes with $w^{(a)} + w^{(b)} = 1$ and $w^{(a)}, w^{(b)} > 0$ (See (21) later in Section IV for how the weights are selected). Notably, we also maintain an $|\mathbf{L}_{1:k}^{(a)}| \times |\mathbf{L}_{1:k}^{(b)}|$ *matched history* matrix $\Xi_{1:k}^{(a,b)}$ (line 4 in Algorithm 1) whose elements are the number of instances that track $i^{(m)} \in \{1, \ldots, |\mathbf{L}_{1:k}^{(a)}|\}$ is matched with track $i^{(n)} \in \{1, \ldots, |\mathbf{L}_{1:k}^{(b)}|\}$. Here, $\mathbf{L}_{1:k}^{(a)}$ is the label space up to time k at node a (likewise for $\mathbf{L}_{1:k}^{(b)}$ at node b). We describe in Algorithm B.2 in Appendix B the method for updating the matched history matrix.

Step 2) Retain unmatched labelled state estimates: We retain the set $\mathbf{X}_k^{(a,\text{ret})}$ of unmatched labelled state estimates at node a (likewise for $\mathbf{X}_k^{(b,\text{ret})}$ at node b) whose lengths exceed a given $\mathcal{C}_{\text{len}}$, *i.e.*,

$$
\mathbf{X}_k^{(a,\text{ret})} = \{\mathbf{a}^{(m)}(k) : m \in \{1, \ldots, |\mathbf{T}_k^{(a)}|\} \setminus Q_k^{(a)}, |\mathcal{D}^{(\mathbf{a}^{(m)})}| \geq \mathcal{C}_{\text{len}}\}.
\tag{16}
$$

Further, any unmatched tracks with lengths less than $\mathcal{C}_{\text{len}}$ are discarded.

3) Compute consensed labelled state estimates: We compute the set $\mathbf{X}_k^{(a,\text{con})}$ of consensed labelled state estimates at node a by combining two components: *i)* the matched and fused labelled state estimates, *ii)* the unmatched and retained labelled state estimates of two nodes, *i.e.*,

$$
\mathbf{X}_k^{(a,\text{con})} = \bar{\mathbf{X}}_k^{(a)} \cup \mathbf{X}_k^{(a,\text{ret})} \cup \mathbf{X}_k^{(b,\text{ret})}.
\tag{17}
$$

Remark 4. The consensed labelled multi-object state estimate $\mathbf{X}_k^{(a,\text{con})}$ does not play a role in optimal matching at the next time step and is used for reporting purposes only. The local multi-object state estimate $\mathbf{X}_{k+1}^{(a)}$ at the next time step $k + 1$ is independent of $\mathbf{X}_k^{(a,\text{con})}$. The optimal matching at $k + 1$ only depends on sets of live tracks $\mathbf{T}_{k+1}^{(a)}$ and $\mathbf{T}_{k+1}^{(b)}$, not on the consensed multi-object state estimate $\mathbf{X}_k^{(a,\text{con})}$.

D. Kinematic consensus for multiple nodes

The previous subsections presented a new kinematic consensus algorithm for fusing multi-object state estimates between two nodes. We now extend the algorithm to more than two nodes. A direct extension results in an $|\mathcal{N}|$-dimensional optimal assignment for the track matching, an NP-hard problem. A

---

[2]When we say track t is observed at node a means that node a declares track t exist.

[3]We implement a naive solution here such that the fused label is the label of the node performing the fusion steps while further improvements to achieve label consensus are discussed in Section III-E. Here, we employ a simple weighted average of the local estimates,

widely used sub-optimal strategy to circumvent this intractable problem is to perform pair-wise matching sequentially [13], [15], [33]. Based on the proposed network architecture in Section II-A, the kinematic consensus is realised in Algorithm 2, called TC-OSPA$^{(2)}$. Algorithm 2 consists of two steps:

Step 1) Fuse each neighbour node with current node: Each neighbour labelled multi-object state estimate is fused to the labelled multi-object state estimate of the node of interest to ensure that only unmatched labelled state estimates with the track lengths greater than or equal to $\mathcal{C}_{\text{len}}$ are retained.

Step 2) Fuse the consensed labelled state estimates sequentially: The consensed labelled state estimates of neighbouring nodes and the nodes of interest are combined sequentially without the track length constraint (*i.e.*, $\mathcal{C}_{\text{len}} = 1$) to retain all unmatched tracks because the label consensus has not been reached.

Algorithm 2 FuseMultiNodes

Input: $\{\mathbf{T}_k^{(a)}\}_{a \in \mathcal{N}}$; $\{\Xi_{1:k-1}^{(a,b)}\}_{a,b \in \mathcal{N}}$; $\{\mathbf{L}_{1:k-1}^{(a)}\}_{a \in \mathcal{N}}$;
Output: $\{\mathbf{X}_k^{(a,\text{con})}\}_{a \in \mathcal{N}}$; $\{\Xi_{1:k}^{(a,b)}\}_{a,b \in \mathcal{N}}$; $\{\mathbf{L}_{1:k}^{(a)}\}_{a \in \mathcal{N}}$;
1: **for** $a = 1 : |\mathcal{N}|$ **do**
2:   $\mathcal{B} := \{1 : |\mathcal{N}|\} \setminus \{a\}$;
3:   $\mathbf{X}_{\text{temp}} = []$;   ▷ Initialise a temporarily consensed labelled multi-object state estimate.
4:   **for** $i = 1 : |\mathcal{B}|$ **do**
       ▷ Step 1: fuse each neighbour node with current node.
5:     $b := \mathcal{B}(i)$;
6:     $[\mathbf{X}_{\text{temp}}^{(i)}, \Xi_{1:k}^{(a,b)}, \mathbf{L}_{1:k}^{(a)}, \mathbf{L}_{1:k}^{(b)}] :=$
7:     FuseTwoNodes$(\mathbf{T}_k^{(a)}, \mathbf{T}_k^{(b)}, \Xi_{1:k-1}^{(a,b)}, \mathbf{L}_{1:k-1}^{(a)}, \mathbf{L}_{1:k-1}^{(b)}, \mathcal{C}_{\text{len}})$;
8:   **end for**
9:   $\mathbf{X}_k^{(a,\text{con})} := \mathbf{X}_{\text{temp}}^{(1)}$;
10:   **if** $|\mathcal{B}| > 1$ **then**
       ▷ Step 2: fuse the consensed labelled state estimates sequentially.
11:     **for** $i = 2 : |\mathcal{B}|$ **do**
12:       $\mathbf{X}_k^{(a,\text{con})} :=$ FuseTwoNodes$(\mathbf{X}_k^{(a,\text{con})}, \mathbf{X}_{\text{temp}}^{(i)}, [], [], [], 1)$;
13:     **end for**
14:   **end if**
15:   $\mathbf{L}_{a,k}^{\text{con}} :=$ UpdateLabels$(\mathcal{L}(\mathbf{X}_k^{(a,\text{con})}); \{\Xi_{1:k}^{(a,b)}\}_{a,b \in \mathcal{N}}; \{\mathbf{L}_{1:k}^{(a)}\}_{a \in \mathcal{N}})$;
16: **end for**

Algorithm 2 (TC-OSPA$^{(2)}$) can be implemented in real-time given the significantly low message sizes realised by transmitting labelled multi-object state estimates compared to transmitting labelled multi-object densities. In particular, suppose that $|\mathbf{T}_{\text{max}}|$ is the maximum number of objects seen by the network, *i.e.*, $|\mathbf{T}_{\text{max}}| = \max\left(|\mathbf{T}^{(1)}|, \ldots, |\mathbf{T}^{(|\mathcal{N}|)}|\right)$, then the order of magnitude of data that needs to be shared is upper bounded by[4]

$$|\mathcal{N}||\mathbf{T}_{\text{max}}|. \tag{18}$$

For example, if $|\mathcal{N}| = 20$ nodes, $|\mathbf{T}_{\text{max}}| = 100$ objects, and each labelled state estimate has 6 dimensions (4 for 2D environments of kinematic state and 2 for the local label's dimension), and each dimension is represented by an 8-byte floating-point value. The maximum amount of data that needs to be shared by a node at one time is 93.75 KB, which is reasonably low to track a large number of objects using 20 distributed nodes. Notably, our method does not require

---

[4]The upper bound is only reached in the case that all nodes observe all the objects. In reality, because of limited FoV sensors, this upper bound will not be reached in most cases.

transmitting all the trajectories because the state estimates from other nodes can be stored in each local node. Even if the trajectories need to be sent, for instance, due to limited memory at each local node, the proposed method only needs to transmit truncated trajectories (*e.g.*, 10 scans). Consequently, the bandwidth needed is much smaller than sending a multi-object density and is proportional to the number of objects. Further, the computational complexity of Algorithm 2 at each local node is $\mathcal{O}(|\mathcal{N}||\mathbf{T}_{\text{max}}|^4 d)$ where d is the dimension of a single-object state. Thus, the computational complexity only increases linearly with respect to the number of nodes. See numerical experiments in Sec. IV for fusing time.

Remark 5. Since our approach is agnostic to local multi-object tracking techniques, we do not assume that the nodes also provide covariances of their estimates. Nonetheless, if the local trackers can provide covariances, then our approach is also applicable by fusing the means and covariances. In particular, we can: i) compute the distance in (2) using the Mahalanobis distance between two Gaussian distributions; ii) compute the fused estimate in (15) and its covariance using methods such as the optimal fusion method for two-sensors [67] or GCI for multiple sensors.

E. Label consensus for multiple objects

The previous subsections address multiple limited FoVs *kinematic consensus*. However, MOT concerns not only the object's positions (kinematic) but also the object's identities (labels). In this subsection, we present our *label consensus* solution that reduces the occurrences of label inconsistency. During the fusion steps, the unmatched and retained labelled state estimates are included in the consensed labelled multi-object state estimates (see (17)). Hence, care must be taken to ensure mismatched labels between nodes are resolved to achieve *label consensus*, as illustrated in the following example.

Example 1. Consider using a two-node distributed sensor network to track a mobile object that follows a constant velocity model over a $[-500, 1500]$m $\times [0, 1000]$m area. The locations of the two nodes are $[0, 400]^T$ m and $[0, 800]^T$ m, respectively. Each node runs an LMB filter locally, and its sensor can only detect objects within its relative angle $[-60°, 60°]$ with detection probability $P_D = 0.98$ and detection range $r_D = 800$ m (see Fig. 3). After the kinematic consensus steps, we have the two following label inconsistency problems:

1) Label inconsistency of the unmatched and retained labelled state estimates. Fig. 3a depicts the consensed labelled state estimates *at node* 1. Although the kinematic fusion successfully helps node 1 track the object, a track fragmentation still occurs even when it moves out of node 1's FoV. This happens because it is no longer detected by node 1, and the network relies on detection information from node 2 (including node 2's label) to track it. Since node 2 has a different label (in red) to the one observed by node 1 (in blue), the consensed labelled state estimates yield two different labels for the same object.
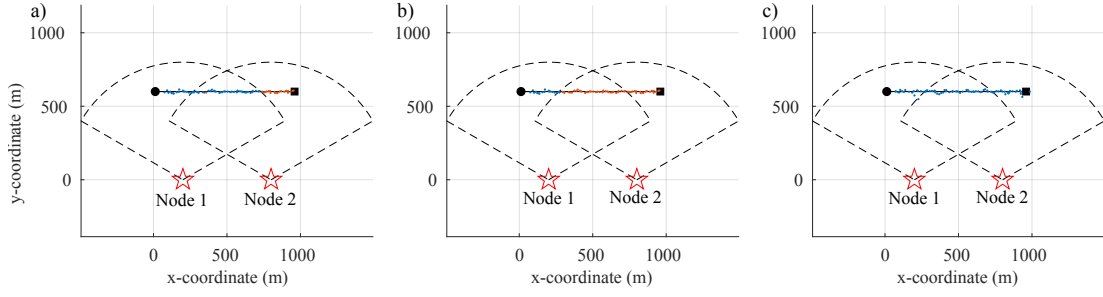
Fig. 3. Example 1 — two nodes with limited FoVs tasked with tracking objects. a) Consensed labelled state estimates at node 1 before reaching label consensus; b) Consensed labelled state estimates at node 2 before reaching label consensus; c) Consensed labelled state estimates at node 1 (likewise for node 2) after reaching label consensus. Here: '$\circ$' is the location of the object's birth; '$\square$' is the location of the object's death. Colour coding represents labels of the objects.

2) Label inconsistency of the matched labelled state estimates. Fig. 3b depicts the consensed labelled state estimates *at node 2*. Initially, the object is not detected by node 2; hence, the network relies on the information from node 1 (including node 1's label in blue) to track it. When the object moves into node 2's FoV, node 2 assigns it a new label in red. During the fusion steps (see (15)), the object is assigned the red label of node 2 (since the fusion is performed at node 2). As a result, the consensed labelled state estimates have different labels for the same object.

In the following, we present a label consensus solution to reduce label inconsistency. The main idea is to construct a graph that represents connections among labels based on the match history matrices $\Xi_{1:k}^{(a,b)}$ whose (m,n) entry is the number of instances the mth track in node a's track-list is matched with the nth track in node b's track-list. In particular, let $G = (V, E)$ be a graph, where:

- the set V of labels is the set of vertices of the graph;
- E is the set of edges representing matches between labels.

Since label consistency requires the same object to have the same label across all nodes of the network (Remark 2), all of the connected vertices should be assigned the same label. For this so-called consensed label, we propose to use the least label of connected vertices according to a lexicographical order of time of birth and unique node ID :

$$\boldsymbol{\ell} = ((k,i),a) < \boldsymbol{\ell}' = ((k',i'),b)$$
$$\Leftrightarrow \quad (k = k') \text{ and } (a < b) \text{ or } (k < k'). \quad (19)$$

The proposed label consensus is provided in Algorithm B.3 in Appendix B, which is used in line 15 of Algorithm 2. Fig. 3c depicts the consensed labelled multi-object state estimate at node 1 after label consensus is achieved. Observe that label inconsistency is eliminated.

IV. NUMERICAL EXPERIMENTS

In this section, we apply the proposed TC-OSPA$^{(2)}$ fusion method[5] to investigate and compare with other fusion strategies in three distributed sensor network settings of increasing complexity. A 2-dimensional search area is adopted for these three scenarios to demonstrate the effectiveness of our method. Each detected object with kinematic state $x = [p_x, \dot{p}_x, p_y, \dot{p}_y]^T$

[5] see *https://github.com/AdelaideAuto-IDLab/Distributed-limitedFoV-MOT* for our open source code release with detailed implementation.

results in an observation z of noisy xy-coordinate positions, given by: $z = [p_x, p_y]^T + v$. Here, $v \sim N(0,R)$ is a 2×1 zero-mean Gaussian process noise with $R = \mathrm{diag}(\sigma_x^2, \sigma_y^2)$ where $\sigma_x = \sigma_y = 10$ m. Each object follows a constant velocity model given by $x_k = F^{CV} x_{k-1} + q_{k-1}^{CV}$. Here, $F^{CV} = [1, T_0; 0, T_0] \otimes I_2$, T_0 is the sampling interval ($T_0 = 1$ s for our experiments), $\otimes$ denotes for the Kronecker tensor product; I_2 is the 2×2 identity matrix; $q_{k-1}^{CV} \sim N(0, Q^{CV})$ is a 4×1 zero-mean Gaussian process noise, with co-variance $Q^{CV} = \sigma_{CV}^2 [T_0^3/3, T_0^2/2; T_0^2/2, T_0] \otimes I_2$ where $\sigma_{CV} = 5$ m/s^2. Each object has survival probability $P_S = 0.98$. Clutter follows a Poisson model with an average of 10 clutters per scan. We use OSPA and OSPA$^{(2)}$ as well as fusing time to measure performance. For OSPA and OSPA$^{(2)}$, we set cut-off $c = 100$ m, order $p = 1$. The OSPA$^{(2)}$ distance at time k is calculated over a 10-scan window ending at k. The fusing time reported is the average execution time for the fusion steps over 100 MC runs—notably, this excludes the execution of the filtering algorithm.

For a fair comparison with LM-GCI in [15], we use an LMB filter at each local node, *although our approach can be used with different filters* such as MHT or GLMB since our method is agnostic to the filters at each node. The LMB filter is implemented with Gaussian mixtures using Gibbs sampling [68] for a joint prediction and update step. The existence threshold is set at 10^{-3}, *i.e.*, any Bernoulli component with label ℓ and its existence probability $r^{(\ell)} < 10^{-3}$ is pruned. A Bernoulli component with label ℓ with existence probability $r^{(\ell)} > 0.5$ is confirmed as an existing object, and its state estimates are extracted from the corresponding state density. Further, we implement the Adaptive Birth Procedure (ABP) in [25]. In particular, the birth distribution $\boldsymbol{\pi}_{B,k+1}$ at time $k + 1$ is a function of measurement sets Z_k, *i.e.*, $\boldsymbol{\pi}_{B,k+1} = \{r_{B,k+1}^{(\ell)}(z), p_{B,k+1}^{(\ell)}(x|z)\}_{l=1}^{|Z_k|}$, where

$$r_{B,k+1}^{(\ell)}(z) = \min\left(r_{B,\max}, \frac{1 - r_{U,k}(z)}{\sum_{\zeta \in Z_k} 1 - r_{U,k}(\zeta)} \lambda_{B,k+1}\right).$$

Here, $r_{U,k}(z)$ is the probability that the measurement z is associated with tracking hypotheses given by

$$r_{U,k}(z) = \sum_{I_{k-1}, \xi, I_k, \theta_k} 1_{\theta_k}(z) w^{(I_{k-1}, \xi)} w^{(I_{k-1}, \xi, I_k, \theta_k)}, \quad (20)$$

where $w^{(I_{k-1}, \xi)} w^{(I_{k-1}, \xi, I_k, \theta_k)}$ is in [68, eq.14], $\lambda_{B,k+1}$ is the expected number of births at time $k + 1$ and $r_{B,\max}$ is the

maximum existence probability of a newly born object. In three scenarios, we set $\lambda_{B,k+1} = 0.5$ and $r_{B,\max} = 0.03$.

For data fusion, since we do not focus on the weight selection problem, the Metropolis weight [69] is implemented, *i.e.*, for each node $a, b \in \mathcal{N}$,

$$ w^{(a,b)} = \begin{cases} \frac{1}{1+\max(|\mathcal{N}^{(a)}|, |\mathcal{N}^{(b)}|)}, & a \in \mathcal{N}, b \in \mathcal{N}^{(a)}, \\ 1 - \sum_{b \in \mathcal{N}^{(a)}} w^{(a,b)}, & a \in \mathcal{N}, b = a. \end{cases} \quad (21) $$

We compare the proposed fusion method TC-OSPA$^{(2)}$, with CA-PHD-GCI [40] and LM-GCI [15]. We also compare our proposed approach with the OSPA metric replaced by the *Wasserstein* metric, here on referred to as TC-WASS. The Wasserstein metric of (integer) order $p \geq 1$ is defined as [70]:

$$ d_{\mathtt{W}}^{(p)}(X,Y) \triangleq \min_{\bar{C}} \Big(\sum_{i=1}^{m} \sum_{j=1}^{n} \bar{C}_{i,j} d(x^{(i)}, y^{(j)})^p \Big)^{1/p} \quad (22) $$

where $\bar{C} = (\bar{C}_{i,j})$ denotes an $m \times n$ transportation matrix, *i.e.*, the entries $\bar{C}_{i,j}$ are non-negative, each row sum to $1/m$, and each column sum to $1/n$. The integer p determines the sensitivity of the metric to outliers in the finite subsets X and Y. Notably, *the Wasserstein distance is undefined if one of the finite subsets is empty*. Consequently, unlike the OSPA track-to-track distance in (2), the time-average (track-to-track) Wasserstein distance between two tracks is undefined if one track is fragmented (as shown in Fig. 2). One method to define a Wasserstein track-to-track distance is to embed the time information as a part of multi-object state: for any $t, u \in \mathbb{T}$, we form finite sets $\tilde{X}^{(t)} = \{(t(k), \alpha k) : k \in \mathcal{D}^{(t)}\}$ and $\tilde{X}^{(u)} = \{(u(k), \alpha k) : k \in \mathcal{D}^{(u)}\}$ and define

$$ \tilde{d}_W(t, u) = d_W^{(p)}(\tilde{X}^{(t)}, \tilde{X}^{(u)}), \quad (23) $$

where α is a user-defined parameter to calibrate the influence of time on the overall distance. In our experiments, we set $\alpha = 20$ m/s—the maximum velocity of all objects. Notably, for the CA-PHD-GCI fusion strategy, the underlying PHD filter does not report labels for multi-object state estimates; hence, tracking performance—in terms of OSPA$^{(2)}$—cannot be assessed. Thus, we only report OSPA for CA-PHD-GCI and use blue to represent estimated object locations without labels in Fig. 4b and Fig. 6b.

A. Scenario 1 — two nodes with a small number of objects

In this setting, we investigate the simple problem of tracking three mobile objects using two sensor nodes with limited FoV sensors in a $[-500, 1500]$ m $\times [0, 800]$ m area. The two nodes are located at $[0, 400]^T$ m and $[0, 800]^T$ m, respectively. At each node, the sensor can only detect objects within its relative angle of $[-50°, 50°]$ with $P_D = 0.98$ and $r_D = 800$ m. This scenario's duration is 80 s, with object 1 and object 2 staying alive for the whole period, while object 3 is born at time 10 s and dies at time 60 s. The track consensus is performed over 5 scans, with track length threshold $\mathcal{C}_{\text{len}} = 2$, *i.e.*, only unmatched tracks with lengths exceeding 2 are retained. The considered scenario setting is shown in Fig. 4a.

Fig. 4, Fig. 5 and Table II compare results across CA-PHD-GCI, LM-GCI, TC-WASS, and TC-OSPA$^{(2)}$ fusion methods.

TABLE II
SCENARIO 1 RESULTS COMPARISON OVER 100 MONTE CARLO RUNS

Strategies	OSPA (m)	OSPA$^{(2)}$ (m)	Fusing time (s)
CA-PHD-GCI	46.6	-	0.383
LM-GCI	31.7	38.8	0.079
TC-WASS	19.6	29.7	0.013
TC-OSPA$^{(2)}$	**19.0**	**27.0**	**0.011**

The results confirm that our proposed TC-OSPA$^{(2)}$ method can accurately detect and track all three objects with consistent labels whilst consuming the shortest fusing time. Due to the small number of objects, TC-WASS also attains a low OSPA error; however, TC-WASS occasionally fails to assign correct labels and results in a higher OSPA$^{(2)}$ error as seen in Table II. In contrast, LM-GCI can only detect and track objects accurately within a sensor's own FoV. After the 30 s duration mark, all three objects are within the intersection of the two sensors' FoVs, and we can observe Node 2 to correctly track all three objects as illustrated in Fig. 5a and 5c. Further, although CA-PHD-GCI can estimate most of these three objects, its accuracy based on the OSPA distance is the poorest because the underlying PHD filter does not perform as well as the LMB filter at each local node [71].

B. Scenario 2 — two nodes with a large number of objects

In this scenario, we consider a more challenging problem using two limited-FoV sensor nodes to track a time-varying and an unknown number of mobile objects in a $[-500, 1800]$ m $\times [-100, 1000]$ m surveillance area. The two nodes are located at $[300, -100]^T$ m and $[1000, -100]^T$ m, respectively. Each sensor can only detect objects within its limited FoV defined by a relative angle of interval $[-50°, 50°]$ with $P_D = 0.98$ and detection range $r_D = 1000$ m. This scenario's duration is 80 s, with various birth and death events and a maximum of 22 objects. The track consensus between two nodes is performed over 5 scans, with track length threshold $\mathcal{C}_{\text{len}} = 2$. The considered scenario is illustrated in Fig. 6a.

Fig. 6b-d depict the consensed labelled multi-object state estimates and the true trajectories at sensor node 2 of a particular run for CA-PHD-GCI, LM-GCI, TC-WASS and TC-OSPA$^{(2)}$, respectively. The results confirm that TC-OSPA$^{(2)}$ successfully detects and tracks all objects without any label inconsistency, regardless of whether objects are in the node's FoV or not. In contrast, LM-GCI can only detect and track most of the objects within the node's FoV. Although CA-PHD-GCI can detect all objects, even those outside the node's FoV, CA-PHD-GCI demonstrates the worst estimation performance as shown in Table III. Fig 7c shows the cardinality estimates; the evidence therein further supports the above observation. It is expected that LM-GCI fails to detect all of the objects compared to CA-PHD-GCI, TC-WASS and TC-OSPA$^{(2)}$ since only the latter three strategies are designed to cope with limited FoV sensors.

Fig. 7a-d and Table III present the performance comparisons among the four fusion strategies in terms of OSPA, OSPA$^{(2)}$ and fusing time over 100 Monte Carlo runs. We can see that TC-OSPA$^{(2)}$ outperforms other fusion strategies, including our
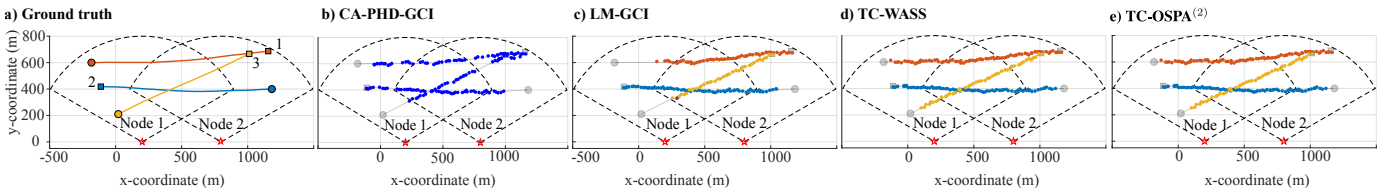
Fig. 4. Scenario 1 ground-truth and consensed labelled multi-object state estimates at sensor node 2: a) ground-truth; b) CA-PHD-GCI (unlabelled approach); c) LM-GCI; d) TC-WASS; e) TC-OSPA$^{(2)}$. Starting and stopping positions are denoted by ∘ and □, respectively. Colour coding represents objects' labels.
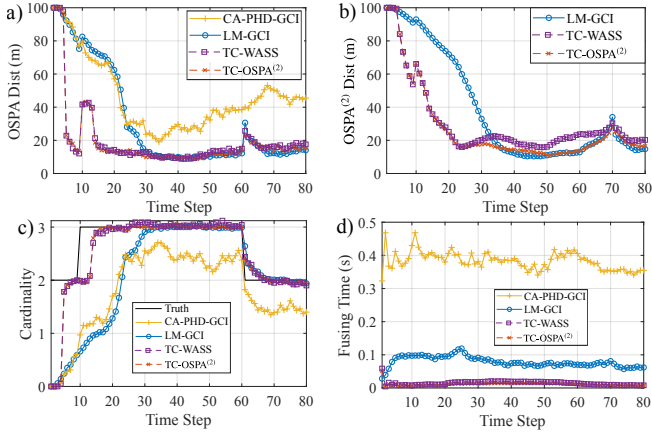

Fig. 5. Comparison results for Scenario 1: a) OSPA distance; b) OSPA$^{(2)}$ distance; c) Cardinality estimations; d) Fusing times.

TABLE III
SCENARIO 2 COMPARISON RESULTS OVER 100 MONTE CARLO RUNS

Strategies	OSPA (m)	OSPA$^{(2)}$ (m)	Fusing time (s)
CA-PHD-GCI	51.5	-	1.095
LM-GCI	42.9	50.1	0.359
TC-WASS	28.6	45.6	0.078
TC-OSPA$^{(2)}$	**21.0**	**32.5**	**0.052**

TABLE IV
PERFORMANCE COMPARISON FOR DIFFERENT P_D VALUES OBTAINED
OVER 100 MONTE CARLO RUNS FOR EACH P_D SETTING AND METHOD

	P_D	CA-PHD-GCI	LM-GCI	TC-WASS	TC-OSPA$^{(2)}$
OSPA (m)	0.7	78.9	61.1	39.9	**37.1**
	0.8	71.1	52.4	34.5	**30.0**
	0.9	64.4	44.7	31.1	**24.1**
OSPA$^{(2)}$ (m)	0.7	-	67.4	55.7	**49.3**
	0.8	-	59.6	51.8	**42.4**
	0.9	-	52.3	48.3	**35.9**

track consensus fusion strategy employed with the adaptation of the Wasserstein metric (TC-WASS) by large margins whilst requiring the shortest fusing time. The reason is that TC-OSPA$^{(2)}$ minimises label inconsistency for limited FoV sensors while fusing the most certain object state estimates within a sensor's FoV (local labelled multi-object state estimates) to reach consensus in both position and label estimations.

Table IV further compares the performance of TC-OSPA$^{(2)}$ with LM-GCI, CA-PHD-GCI, and TC-WASS under different detection probability, P_D, settings. It is expected that the occurrences of label inconsistency will increase when P_D decreases. Consequently, the tracking accuracy decreases when P_D decreases, concurring with our observation in Remark 3. Nevertheless, the results in Table IV show the proposed TC-OSPA$^{(2)}$ approach to consistently outperform the other three fusion strategies across the P_D values.
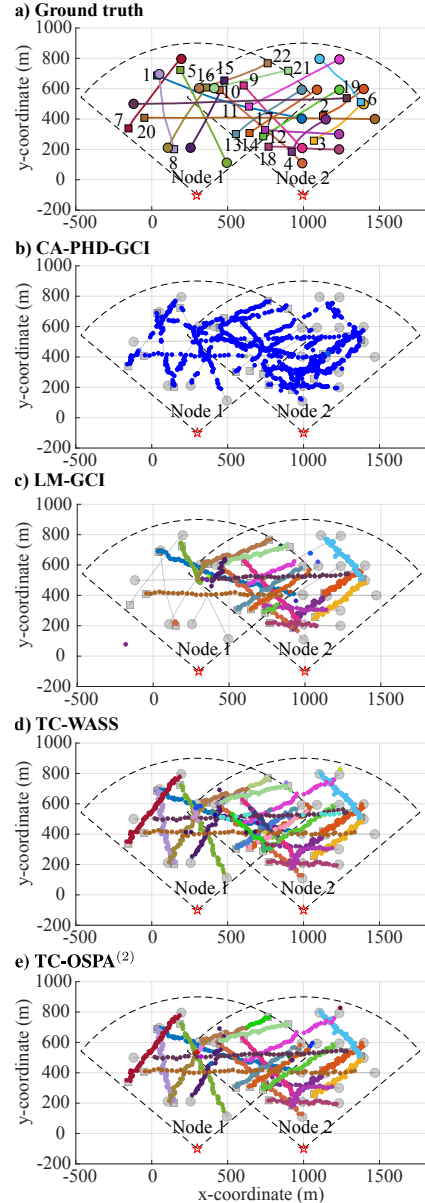

Fig. 6. Scenario 2 ground-truth and consensed labelled multi-object state estimates at sensor node 2: a) ground-truth; b) CA-PHD-GCI (unlabelled approach); c) LM-GCI; d) TC-WASS; e) TC-OSPA$^{(2)}$. Starting and stopping positions are denoted by ∘ and □, respectively. Colour coding represents labels of the objects. Although less apparent, several false tracks are visible in the region of $[500, 1000]$ m $\times[200, 600]$ m in Fig. 6d when using TC-WASS.

C. Scenario 3 — a large number of nodes

To further demonstrate our proposed fusion method's effectiveness, we consider a scenario with 16 limited FoV sensor nodes for tracking a time-varying and unknown number of mobile objects in a $[-1000, 1000]$ m $\times$ $[-1000, 1000]$ m surveillance area. These 16 nodes are positioned near the edge of the area. Each sensor can only detect objects within its

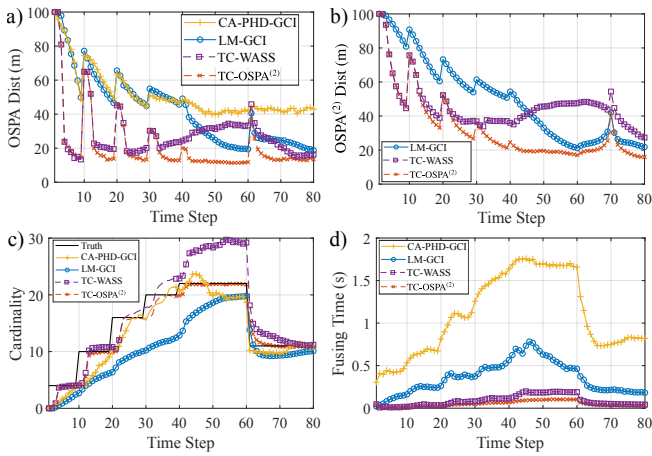Fig. 7. Comparison results for Scenario 2: a) OSPA distance; b) OSPA$^{(2)}$ distance; c) Cardinality estimations; d) Fusing times.
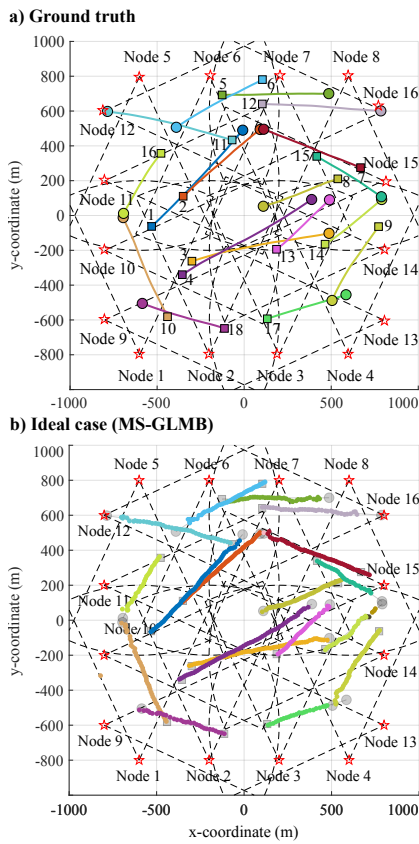

Fig. 8. Scenario 3 — a) ground-truth; b) ideal case (MS-GLMB—centralised method where all of the sensor FoVs are completely known). Starting and stopping positions are denoted by ○ and □, respectively. Colour coding represents objects' labels.

limited FoV defined by a relative angle of interval $[-25°, 25°]$ with $P_D = 0.98$ and detection range $r_D = 1000$ m. This scenario's duration is 75 s with various birth, death events and a maximum of 18 objects. Further, due to higher uncertainty, the track consensus is performed over 10 scans (instead of 5 as in Scenario 2), with a track length threshold $C_{\text{len}} = 4$. The scenario described is depicted in Fig. 8a. Notably, for this scenario, we can only compare TC-OSPA$^{(2)}$ with TC-WASS and LM-GCI since it is unclear how CA-PHD-GCI can be implemented for more than two nodes. Additionally, we implement MS-GLMB in [72] for this scenario (see Fig. 8b)
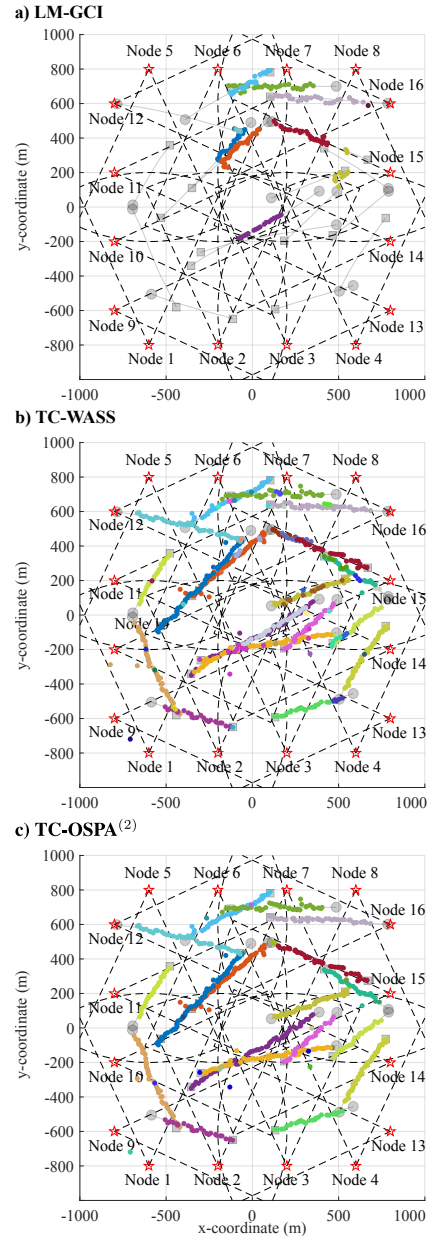

Fig. 9. Scenario 3 — consensed labelled multi-object state estimates at sensor node 7: a) LM-GCI; b) TC-WASS; c) TC-OSPA$^{(2)}$. Starting and stopping positions are denoted by ○ and □, respectively. Colour coding represents objects' labels.

as a lower bound (*ideal case*) on the estimation error, *i.e.* to show how close/far of our proposed fusion method is from the ideal case of centralised tracking when all of the sensors' FoVs are known.

Fig. 9a-c depict the consensed labelled multi-object state estimates and the ground-truth at node 7 for LM-GCI, TC-WASS and TC-OSPA$^{(2)}$, respectively, for one particular execution. Although LM-GCI detects a few objects outside of node 7's FoV, many objects are missed because LM-GCI is not designed for partially overlapped sensor FoV situations. In contrast, TC-WASS and TC-OSPA$^{(2)}$ employing our track consensus-based fusion method can detect, track and assign correct labels for most of the objects, regardless of the objects' locations. The cardinality estimates further confirm the results
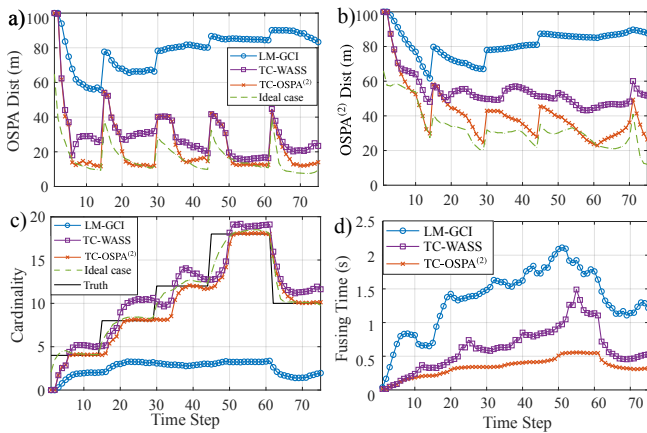
Fig. 10. Comparison results at node 7 for Scenario 3: a) OSPA distance; b) OSPA$^{(2)}$ distance; c) Cardinality estimations; d) Fusing times.

TABLE V
SCENARIO 3 COMPARISON RESULTS OVER 100 MONTE CARLO RUNS

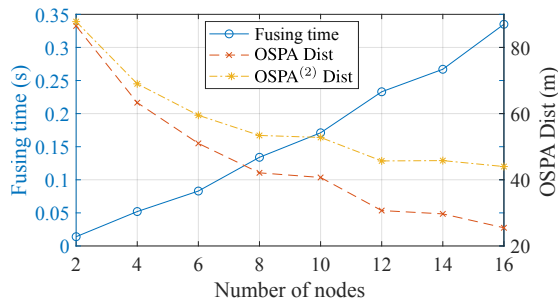| Strategies	OSPA (m)	OSPA$^{(2)}$ (m)	Fusing times (s)
LM-GCI	78.7	81.6	1.35
TC-WASS	30.2	54.4	0.62
TC-OSPA$^{(2)}$	**23.7**	**41.3**	**0.34**
Ideal case (centralised method)	16.6	32.7	-

Fig. 11. TC-OSPA$^{(2)}$ tracking performance at sensor node 2 for Scenario 3 over 100 MC runs when the number of nodes is increased from 2 to 16 (*i.e.*, the number of communications from peer nodes at node 2 is increased from 1 to 15) whilst the ground truth is maintained as shown in Fig. 8a.

plotted in Fig. 10c, which demonstrates that TC-OSPA$^{(2)}$ and TC-WASS can detect and track all 18 objects in this scenario. In comparison, LM-GCI can only detect up to 4 objects on average, over 100 MC runs.

Fig. 10a-d provide detailed tracking performance comparisons, not easily visible in Fig. 9. The results further demonstrate the robustness of TC-OSPA$^{(2)}$. It significantly outperforms LM-GCI and TC-WASS across three performance metrics: OSPA, OSPA$^{(2)}$ and fusing time. Table V summarises performance comparison results confirming the effectiveness of our proposed distributed fusion strategy. It also demonstrates that the performances of our distributed fusion method closely approach the performance of the centralised method.

Fig. 11 plots the overall tracking performance at sensor node 2 in Scenario 3 for TC-OSPA$^{(2)}$ as the number of nodes is increased from 2 to 16 (*i.e.*, the number of communications from peer nodes at node 2 is increased from 1 to 15)

whilst maintaining the same ground truth as in Fig. 8a. The results validate the scalability of our proposed fusion strategy, wherein the fusing time increases linearly with respect to the number of nodes, *i.e.*, $\mathcal{O}(|\mathcal{N}|)$. Even with 16 nodes, the fusing time is relatively short, suitable for real-time tracking in several applications. As expected, when the number of nodes increases, the OSPA and OSPA$^{(2)}$ errors decrease since the nodes can benefit from shared local labelled multi-object state estimates of other nodes to complement their own limited FoVs, thereby improve coverage area, and tracking accuracy.

V. CONCLUSION

A new scalable DMOT solution for multi-sensors with limited FoV sensors has been proposed. Our solution consists of a novel track consensus algorithm coupled with a label consensus method based on the OSPA$^{(2)}$ metric. The better efficiency and accuracy of the proposed DMOT solution are due to the fusion of multi-object state estimates using track consensus over several scans, whereas current solutions fuse multi-object densities from a single scan. Experimental results demonstrate improvements in both speed and accuracy over current methods.

Importantly, our DMOT approach does not rely on any specific tracking methodology but only requires that each node provide a set of estimated tracks. Hence, it provides the flexibility for different network nodes to run different MOT algorithms, which is often the case in heterogeneous and ad-hoc networks.

APPENDIX

A. Mathematical proofs

Proof of Proposition 1: For any $m \in \{1, \dots, N\}$, applying triangle inequality, we have:

$$\tilde{d}^{(c)}(a^{(m)}, b^{(m)}) \leq \tilde{d}^{(c)}(a^{(m)}, u^{(m)}) + \tilde{d}^{(c)}(u^{(m)}, b^{(m)}),$$
$$\leq 2\mathcal{E}. \tag{24}$$

Similarly, using the triangle inequality and the bound $\mathcal{E}$, for any $n, m \in \{1, \dots, N\}$ and $n \neq m$, we have

$$\tilde{d}^{(c)}(a^{(m)}, b^{(n)}) \geq \tilde{d}^{(c)}(u^{(m)}, b^{(n)}) - \tilde{d}^{(c)}(u^{(m)}, a^{(m)}) \tag{25}$$
$$\geq \tilde{d}^{(c)}(u^{(m)}, b^{(n)}) - \mathcal{E},$$
$$\geq \tilde{d}^{(c)}(u^{(m)}, u^{(n)}) - 2\mathcal{E}. \tag{26}$$

Using (8) and $\tilde{d}^{(c)}(u^{(m)}, u^{(n)}) > 4\mathcal{E}$, we have

$$\tilde{d}^{(c)}(a^{(m)}, b^{(n)}) > \tilde{d}^{(c)}(a^{(m)}, b^{(m)}). \tag{27}$$

Using Definition 2 and (7), we have

$$\pi^* = \operatorname*{arg\,min}_{\pi \in \Pi_{|\mathbf{T}_k^{(b)}|}} \sum_{m=1}^{|\mathbf{T}_k^{(a)}|} \tilde{d}^{(c)}(a^{(m)}, b^{(\pi(m))}) \tag{28}$$

$$= \operatorname*{arg\,min}_{\pi \in \Pi_{|\mathbf{T}_k^{(b)}|}} \left[\sum_{m=1}^{N} \tilde{d}^{(c)}(a^{(m)}, b^{(\pi(m))}) + (|\mathbf{T}_k^{(a)}| - N)c \right]. \tag{29}$$

Since $\tilde{d}^{(c)}(a^{(m)}, b^{(\pi(m))}) = c \; \forall \pi(m) > N$ according to (7) and $(|\mathbf{T}_k^{(a)}| - N)c$ is a constant, (29) is equivalent to

$$\pi^* = \arg\min_{\pi \in \Pi_N} J(\pi), \tag{30}$$

where $J(\pi) = \sum_{m=1}^{N} \tilde{d}^{(c)}(a^{(m)}, b^{\pi(m)})$.

Let $\hat{\pi} \in \Pi_N$ be an assignment function that satisfies (4) (*i.e.*, $\hat{\pi}(m) = m \; \forall m \in \{1, \ldots, N\}$). According to Definition 3, if π^* satisfies (4), and we assign the same label to each matched pair, then the N distinct objects have label consistency.

We now prove that $\pi^* = \hat{\pi}$ by using contradiction. Suppose that $\pi^* \neq \hat{\pi}$. Then according to (30), $J(\pi^*) < J(\hat{\pi})$. Thus, $\exists m, n \in \{1, \ldots, N\}$ and $m \neq n$ such that $\pi^*(m) = n$ and $\tilde{d}^{(c)}(a^{(m)}, b^{(n)}) \leq \tilde{d}^{(c)}(a^{(m)}, b^{(m)})$, otherwise we would have $J(\pi^*) > J(\hat{\pi})$. However, $\tilde{d}^{(c)}(a^{(m)}, b^{(n)}) \leq \tilde{d}^{(c)}(a^{(m)}, b^{(m)})$ contradicts (27). Therefore $\pi^* = \hat{\pi}$. ∎

Proof of Proposition 2: From the Definition 4, we have:

$$P_X(a^{(m)}) = \frac{|\mathcal{D}^{(a^{(m)})}|}{n} = P_X^{\min} + \epsilon, \tag{31}$$

where $n = k - j + 1$ and $\epsilon \geq 0$.

Using (2)

$$
\begin{aligned}
\tilde{d}^{(c)}(a^{(m)}, u^{(m)}) &= \sum_{i=j}^{k} \frac{d_0^{(c)}(\{a^{(m)}(i)\}, \{u^{(m)}(i)\})}{n} \\
&= \frac{1}{n} \sum_{i \in \mathcal{D}^{(a^{(m)})}} d_0^{(c)}(\{a^{(m)}(i)\}, \{u^{(m)}(i)\}) + \frac{n - |\mathcal{D}^{(a^{(m)})}|}{n} c \\
&\leq (P_X^{\min} + \epsilon)\varepsilon + (1 - P_X^{\min} - \epsilon)c \\
&\leq \varepsilon P_X^{\min} + (1 - P_X^{\min})c - \epsilon(c - \varepsilon) \\
&\leq \varepsilon P_X^{\min} + (1 - P_X^{\min})c.
\end{aligned}
\tag{32}
$$

Similarly, we have

$$\tilde{d}^{(c)}(b^{(m)}, u^{(m)}) \leq \varepsilon P_X^{\min} + (1 - P_X^{\min})c. \quad ∎$$

B. Pseudocodes

The pseudocode for determining matched pairs based on OSPA$^{(2)}$ distance between two tracks is given in Algorithm B.1. The pseudocode for updating matched history for the matched pairs is given in Algorithm B.2. Lastly, the pseudocode for updating consensed labels to ensure label consistency is given in Algorithm B.3.

1) Determine Matched Pairs — Algorithm B.1: The associated cost C between two sets of tracks is initialised in line 1 based on the size of $\mathbf{T}_k^{(a)}$ and $\mathbf{T}_k^{(b)}$, and thereafter computed in lines $2 - 6$ via the OSPA track-to-track distance in (2). The optimal assignment π^* is computed in line 7 via the Hungarian algorithm. The assignment matrix H^* is initialised based on the size of $\mathbf{T}_k^{(a)}$ and $\mathbf{T}_k^{(b)}$ in line 1 and thereafter computed in lines $8 - 11$ such that only optimal assignments with associated cost less than c (see line 11) are considered as optimal matches. Here, $\odot$ denotes the element-wise product between two matrices. The matched pair matrix Q is computed in lines $12 - 15$ based on the assignment matrix H^*.

Algorithm B.1 DetermineMatchedPairs

Input: $\mathbf{T}_k^{(a)}; \mathbf{T}_k^{(b)};$
Output: $Q_k = [Q_k^{(a)}, Q_k^{(b)}];$
1: $C := \mathsf{zeros}(|\mathbf{T}_k^{(a)}|, |\mathbf{T}_k^{(b)}|); H^* := \mathsf{zeros}(|\mathbf{T}_k^{(a)}|, |\mathbf{T}_k^{(b)}|);$
2: **for** $m = 1 : |\mathbf{T}_k^{(a)}|$ **do**
3:     **for** $n = 1 : |\mathbf{T}_k^{(b)}|$ **do**
4:        $C_{m,n} := \tilde{d}^{(c)}(a^{(m)}, b^{(n)})$ via (2)
5:     **end for**
6: **end for**
7: $\pi^* := \mathsf{OptimalAssignment}(C);$ ▷ Use Hungarian's algorithm.
8: **for** $m = 1 : |\mathbf{T}_k^{(a)}|$ **do**
9:     $H^*_{m, \pi^*(m)} := 1;$
10: **end for**
11: $H^* := H^* \odot (C < c);$ ▷ Select assignments with cost $C < c$.
12: $i_k^{(a)} := [1 : |\mathbf{T}_k^{(a)}|]^T; i_k^{(b)} := [1 : |\mathbf{T}_k^{(b)}|]^T;$
13: $Q_k^{(a)} := i_k^{(a)}; Q_k^{(b)} := H^* \cdot i_k^{(b)}; Q_k := [Q_k^{(a)}, Q_k^{(b)}];$
14: $Q^{\text{check}} := [Q_k^{(a)} \odot Q_k^{(b)}] > 0;$ ▷ Ensure $H^*_{m, \pi^*(m)} = 1.$
15: $Q_k := Q_k(:, Q^{\text{check}});$

---

2) Update Matched History — Algorithm B.2: The matched history matrix $\Xi_{1:k}^{(a,b)}$ at time k is initialised in lines $1-2$ based on the current label spaces of two nodes, and the previous matched history matrix $\Xi_{1:k-1}^{(a,b)}$ at time $k-1$. Line 3 initialises the indices of the label spaces from two node a and b. The matched history matrix $\Xi_{1:k}^{(a,b)}$ is computed in lines $4 - 10$ based on the matched pair matrix $Q_k = [Q_k^{(a)}, Q_k^{(b)}]$ from Algorithm B.1 such that if track $i^{(m)} \in \{1, \ldots, |\mathbf{L}_{1:k}^{(a)}|\}$ from node a (line 7) is matched to track $i^{(n)} \in \{1, \ldots, |\mathbf{L}_{1:k}^{(b)}|\}$ from node b (line 8), then we add 1 into $\Xi_{1:k-1}^{(a,b)}(i^{(m)}, i^{(n)})$ (line 9) to record the number of instances that tracks from node a is matched with track from node b.

Algorithm B.2 UpdateMatchedHistory

Input: $\Xi_{1:k-1}^{(a,b)}; \mathbf{L}_{1:k}^{(a)}; \mathbf{L}_{1:k}^{(b)}; Q_k = [Q_k^{(a)}, Q_k^{(b)}];$
Output: $\Xi_{1:k}^{(a,b)};$
1: $\Xi_{1:k}^{(a,b)} := \mathsf{zeros}(|\mathbf{L}_{1:k}^{(a)}|, |\mathbf{L}_{1:k}^{(b)}|);$
2: $\Xi_{1:k}^{(a,b)}(1 : |\mathbf{L}_{1:k-1}^{(a)}|, 1 : |\mathbf{L}_{1:k-1}^{(b)}|) := \Xi_{1:k-1}^{(a,b)};$
3: $i_{1:k}^{(a)} := 1 : |\mathbf{L}_{1:k}^{(a)}|; i_{1:k}^{(b)} := 1 : |\mathbf{L}_{1:k}^{(b)}|$
4: **for** $i = 1 : |Q_k^{(a)}|$ **do**
5:     $m := Q_k^{(a)}(i); n := Q_k^{(b)}(i);$
6:     $\ell^{(m)} := \mathbf{L}_k^{(a)}(:, m); \ell'^{(n)} := \mathbf{L}_k^{(b)}(:, n);$
7:     $i^{(m)} := i_{1:k}^{(a)}(\ell^{(m)} = \mathbf{L}_{1:k}^{(a)});$
8:     $i^{(n)} := i_{1:k}^{(b)}(\ell'^{(n)} = \mathbf{L}_{1:k}^{(b)});$
9:     $\Xi_{1:k}^{(a,b)}(i^{(m)}, i^{(n)}) := \Xi_{1:k}^{(a,b)}(i^{(m)}, i^{(n)}) + 1;$
10: **end for**

---

3) Update Labels— Algorithm B.3: The graph $G = (V, E)$, which represents the matched history matrices amongst all nodes ($\{\Xi_{1:k}^{(a,b)}\}_{a,b \in \mathcal{N}}$), is created in line 1. Here, $V = 1 : |\{\mathbf{L}_{1:k}^{(a)}\}_{a \in \mathcal{N}}|$ is the set of vertices of the graph, and E is the set of edges representing matches between labels such that if $(i, j) \in E$ then the track $\{\mathbf{L}_{1:k}^{(a)}\}_{a \in \mathcal{N}}(:, i)$ has at least one instance from time 1 to k (based on $\{\Xi_{1:k}^{(a,b)}\}_{a,b \in \mathcal{N}}$) that is matched to track $\{\mathbf{L}_{1:k}^{(a)}\}_{a \in \mathcal{N}}(:, j)$. Each label $\ell \in \mathbf{L}_k^{\text{con}}$ is updated in the main loop from lines $2 - 18$ as follows. The vertex $m \in V$ is computed based on label ℓ in line 4, while the set of all nearest vertices M connected to m is computed in line 5 using the nearest function in MATLAB. From the

set M of all connected vertices to the vertex m, we conduct a search using the inner loop (lines $7-17$) to find the least label from M using lexicographical order defined in (19) (line 10) subject to the label's uniqueness constraint in lines $12-15$.

Algorithm B.3 UpdateLabels

Input: $\mathbf{L}_k^{con}$; $\{\Xi_{1:k}^{(a,b)}\}_{a,b\in\mathcal{N}}$; $\{\mathbf{L}_{1:k}^{(a)}\}_{a\in\mathcal{N}}$;
Output: $\mathbf{L}_k^{con}$;
▷ Create a graph representation using matched history matrices (see label consensus in Section III-E).

1: $G = (V, E) := \mathsf{CreateAGraph}(\{\Xi_{1:k}^{(a,b)}\}_{a,b\in\mathcal{N}})$;
2: **for** $i = 1 : |\mathbf{L}_k^{con}|$ **do**
3:    $\boldsymbol{\ell} := \mathbf{L}_k^{con}(:, i)$;
4:    $m := V(\boldsymbol{\ell} = \{\mathbf{L}_{1:k}^{(a)}\}_{a\in\mathcal{N}})$;
5:    $M := \mathsf{nearest}(G, m)$;   ▷ Get all connected vertices to vertex m.
6:    $count := |M|$;
7:    **while** $count > 0$ **do**
8:      $count := count - 1$;
9:      $\mathbf{L}^{sel} := \{\mathbf{L}_{1:k}^{(a)}\}_{a\in\mathcal{N}}(:, M)$;
     ▷ Get the smallest index using lexicographical order via (19).
10:      $[\sim, n] := \mathsf{min}(\mathbf{L}^{sel})$;
11:      $\boldsymbol{\ell}' = \mathbf{L}^{sel}(:, n)$;
12:      **if** $\boldsymbol{\ell}' \notin \mathbf{L}_k^{con}$ **then**   ▷ Ensure labels' uniqueness.
13:        $\mathbf{L}_k^{con}(:, i) := \boldsymbol{\ell}'$;   ▷ Update the label.
14:        **break**;   ▷ Escape while loop.
15:      **end if**
16:      $M(n) := []$;   ▷ Remove n from the nearest vertices.
17:    **end while**
18: **end for**

REFERENCES

[1] S. Blackman and R. Popoli, *Design and analysis of modern tracking systems*. Artech House, 1999.

[2] J. Mullane, B. Vo, M. D. Adams, and B. Vo, "A random-finite-set approach to Bayesian SLAM," *IEEE Trans. on Robotics*, vol. 27, no. 2, pp. 268–282, April 2011.

[3] H. V. Nguyen, M. Chesser, L. P. Koh, H. Rezatofighi, and D. C. Ranasinghe, "Trackerbots: Autonomous unmanned aerial vehicle for real-time localization and tracking of multiple radio-tagged animals," *J. of Field Robotics*, vol. 36, no. 3, pp. 617–635, 2019.

[4] H. V. Nguyen, F. Chen, J. Chesser, H. Rezatofighi, and D. Ranasinghe, "LAVAPilot: Lightweight UAV trajectory planner with situational awareness for embedded autonomy to track and locate radio-tags," in *Proc. of the IROS 2020*, Oct 2020, pp. 2488–2495.

[5] I. J. Cox and S. L. Hingorani, "An efficient implementation of Reid's multiple hypothesis tracking algorithm and its evaluation for the purpose of visual tracking," *IEEE Trans. on Patt. Analysis and Machine Intel.*, vol. 18, no. 2, pp. 138–150, Feb 1996.

[6] M. Munz, M. Mählisch, and K. Dietmayer, "Generic centralized multi sensor data fusion based on probabilistic sensor and environment models for driver assistance systems," *IEEE Intel. Transport. Systems Magazine*, vol. 2, no. 1, pp. 6–17, Spring 2010.

[7] S. Reuter, A. Danzer, M. Stübler, A. Scheel, and K. Granström, "A fast implementation of the labeled multi-Bernoulli filter using Gibbs sampling," in *IEEE Intel. Veh. Sympo.*, 2017, pp. 765–772.

[8] R. Hoseinnezhad, B.-N. Vo, B.-T. Vo, and D. Suter, "Visual tracking of numerous targets via multi-Bernoulli filtering of image data," *Pattern Recognition*, vol. 45, no. 10, pp. 3625 – 3635, 2012.

[9] S. H. Rezatofighi, S. Gould, B. T. Vo, B.-N. Vo, K. Mele, and R. Hartley, "Multi-target tracking with time-varying clutter rate and detection profile: application to time-lapse cell microscopy sequences," *IEEE Trans. on Medical Imaging*, vol. 34, no. 6, pp. 1336–1348, 2015.

[10] E. L. Souza, E. F. Nakamura, and R. W. Pazzi, "Target tracking for sensor networks: A survey," *ACM Computing Surveys*, vol. 49, no. 2, Jun. 2016.

[11] R. P. Mahler, *Statistical multisource-multitarget information fusion*. Artech House, Inc., 2007, vol. 685.

[12] D. Reid, "An algorithm for tracking multiple targets," *IEEE Trans. on Automatic Control*, vol. 24, no. 6, pp. 843–854, 1979.

[13] G. Battistelli, L. Chisci, C. Fantacci, A. Farina, and A. Graziano, "Consensus CPHD filter for distributed multitarget tracking," *IEEE J. of Sel. Topics in Signal Process.*, vol. 7, no. 3, pp. 508–520, 2013.

[14] G. Battistelli and L. Chisci, "Kullback-Leibler average, consensus on probability densities, and distributed state estimation with guaranteed stability," *Automatica*, vol. 50, no. 3, pp. 707 – 718, 2014.

[15] S. Li, G. Battistelli, L. Chisci, W. Yi, B. Wang, and L. Kong, "Computationally efficient multi-agent multi-object tracking with labeled random finite sets," *IEEE Trans. on Signal Process.*, vol. 67, no. 1, pp. 260–275, 2019.

[16] A. R. Persico, P. Kirkland, C. Clemente, J. J. Soraghan, and M. Vasile, "Cubesat-based passive bistatic radar for space situational awareness: A feasibility study," *IEEE Trans. on Aerosp. Electron. Systems*, vol. 55, no. 1, pp. 476–485, Feb 2019.

[17] Z.-Q. Luo, M. Gastpar, J. Liu, and A. Swami, "Distributed signal processing in sensor networks [from the guest editors]," *IEEE Signal Process. Magazine*, vol. 23, no. 4, pp. 14–15, July 2006.

[18] M. E. Liggins, C.-Y. Chong, I. Kadar, M. G. Alford, V. Vannicola, and S. Thomopoulos, "Distributed fusion architectures and algorithms for target tracking," *Proc. of IEEE*, vol. 85, no. 1, pp. 95–107, Jan 1997.

[19] R. P. Mahler, "Optimal/robust distributed data fusion: a unified approach," in *Signal Process., Sensor Fusion, and Target Recogn. IX*, vol. 4052. Inter. Society for Optics and Photonics, 2000, pp. 128–138.

[20] M. Üney, D. E. Clark, and S. J. Julier, "Distributed fusion of PHD filters via exponential mixture densities," *IEEE J. of Sel. Topics in Signal Process.*, vol. 7, no. 3, pp. 521–531, June 2013.

[21] R. P. S. Mahler, "Multitarget Bayes filtering via first-order multitarget moments," *IEEE Trans. on Aerosp. Electron. Systems*, vol. 39, no. 4, pp. 1152–1178, Oct 2003.

[22] R. Mahler, "PHD filters of higher order in target number," *IEEE Trans. on Aerosp. Electron. Systems*, vol. 43, no. 4, 2007.

[23] B.-T. Vo, B.-N. Vo, and A. Cantoni, "The cardinality balanced multi-target multi-Bernoulli filter and its implementations," *IEEE Trans. on Signal Process.*, vol. 57, no. 2, pp. 409–423, 2009.

[24] J. L. Williams, "An efficient, variational approximation of the best fitting multi-bernoulli filter," *IEEE Trans. on Signal Process.*, vol. 63, no. 1, pp. 258–273, Jan 2015.

[25] S. Reuter, B.-T. Vo, B.-N. Vo, and K. Dietmayer, "The labeled multi-Bernoulli filter," *IEEE Trans. on Signal Process.*, vol. 62, no. 12, pp. 3246–3260, 2014.

[26] B.-T. Vo and B.-N. Vo, "Labeled random finite sets and multi-object conjugate priors," *IEEE Trans. on Signal Process.*, vol. 61, no. 13, pp. 3460–3475, 2013.

[27] B.-N. Vo, B.-T. Vo, and D. Phung, "Labeled random finite sets and the Bayes multi-target tracking filter," *IEEE Trans. on Signal Process.*, vol. 62, no. 24, pp. 6554–6567, 2014.

[28] B.-N. Vo and B.-T. Vo, "A multi-scan labeled random finite set model for multi-object state estimation," *IEEE Trans. on Signal Process.*, vol. 67, no. 19, pp. 4948–4963, 2019.

[29] T. M. Cover and J. A. Thomas, *Elements of information theory*. John Wiley & Sons, 2012.

[30] K.-C. Chang, C.-Y. Chong, and S. Mori, "Analytical and computational evaluation of scalable distributed fusion algorithms," *IEEE Trans. on Aerosp. Electron. Systems*, vol. 46, no. 4, pp. 2022–2034, 2010.

[31] S. J. Julier, T. Bailey, and J. K. Uhlmann, "Using exponential mixture models for suboptimal distributed data fusion," in *Proc. of the IEEE Nonlinear Statistical Signal Process. Workshop*, 2006, pp. 160–163.

[32] D. Clark, S. Julier, R. Mahler, and B. Ristic, "Robust multi-object sensor fusion with unknown correlations," in *Proc. of the Sensor Signal Process. for Defence*, Sep. 2010, pp. 1–5.

[33] C. Fantacci, B.-N. Vo, B.-T. Vo, G. Battistelli, and L. Chisci, "Consensus labeled random finite set filtering for distributed multi-object tracking," *arXiv preprint arXiv:1501.01579*, 2015.

[34] M. B. Hurley, "An information theoretic justification for covariance intersection and its generalization," in *Proc. of the 5th FUSION*, vol. 1, July 2002, pp. 505–511.

[35] B. Wang, W. Yi, R. Hoseinnezhad, S. Li, L. Kong, and X. Yang, "Distributed fusion with multi-Bernoulli filter based on generalized covariance intersection," *IEEE Trans. on Signal Process.*, vol. 65, no. 1, pp. 242–255, 2016.

[36] C. Fantacci, B.-N. Vo, B.-T. Vo, G. Battistelli, and L. Chisci, "Robust fusion for multisensor multiobject tracking," *IEEE Signal Process. Lett.*, vol. 25, no. 5, pp. 640–644, 2018.

[37] S. Li, W. Yi, R. Hoseinnezhad, G. Battistelli, B. Wang, and L. Kong, "Robust distributed fusion with labeled random finite sets," *IEEE Trans. on Signal Process.*, vol. 66, no. 2, pp. 278–293, 2018.

[38] W. Yi, S. Li, B. Wang, R. Hoseinnezhad, and L. Kong, "Computationally efficient distributed multi-sensor fusion with multi-Bernoulli filter," *IEEE Trans. on Signal Process.*, vol. 68, pp. 241–256, 2020.

[39] M. Üney, J. Houssineau, E. Delande, S. J. Julier, and D. E. Clark, "Fusion of finite-set distributions: Pointwise consistency and global cardinality," *IEEE Trans. on Aerosp. Electron. Systems*, vol. 55, no. 6, pp. 2759–2773, Dec 2019.

[40] G. Li, G. Battistelli, W. Yi, and L. Kong, "Distributed multi-sensor multi-view fusion based on generalized covariance intersection," *Signal Process.*, vol. 166, p. 107246, 2020.

[41] T. Li, J. M. Corchado, S. Sun, and J. Bajo, "Clustering for filtering: Multi-object detection and estimation using multiple/massive sensors," *Information Sciences*, vol. 388-389, pp. 172–190, 2017.

[42] T. Li, V. Elvira, H. Fan, and J. M. Corchado, "Local-diffusion-based distributed SMC-PHD filtering using sensors with limited sensing range," *IEEE Sensors Journal*, vol. 19, no. 4, pp. 1580–1589, 2019.

[43] T. Li, J. M. Corchado, and S. Sun, "Partial consensus and conservative fusion of gaussian mixtures for distributed PHD fusion," *IEEE Trans. on Aerosp. Electron. Systems*, vol. 55, no. 5, pp. 2150–2163, Oct 2019.

[44] T. Li, M. Mallick, and Q. Pan, "A parallel filtering-communication-based cardinality consensus approach for real-time distributed PHD filtering," *IEEE Sensors Journal*, vol. 20, no. 22, pp. 13 824–13 832, 2020.

[45] L. Gao, G. Battistelli, and L. Chisci, "Multiobject fusion with minimum information loss," *IEEE Signal Process. Let.*, vol. 27, pp. 201–205, 2020.

[46] T. Li, X. Wang, Y. Liang, and Q. Pan, "On arithmetic average fusion and its application for distributed multi-Bernoulli multitarget tracking," *IEEE Trans. on Signal Process.*, vol. 68, pp. 2883–2896, 2020.

[47] L. Gao, G. Battistelli, and L. Chisci, "Event-triggered distributed multi-target tracking," *IEEE Trans. on Signal and Inf. Process. over Networks*, vol. 5, no. 3, pp. 570–584, Sep. 2019.

[48] C.-Y. Chong, S. Mori, and K.-C. Chang, "Distributed multitarget multisensor tracking," *Multitarget-multisensor tracking: Advanced applications*, pp. 247–296, 1990.

[49] K. C. Chang, R. K. Saha, and Y. Bar-Shalom, "On optimal track-to-track fusion," *IEEE Trans. on Aerosp. Electron. Systems*, vol. 33, no. 4, pp. 1271–1276, 1997.

[50] C.-Y. Chong, S. Mori, W. H. Barker, and K.-C. Chang, "Architectures and algorithms for track association and fusion," *IEEE Aerospace and Electronic Systems Magazine*, vol. 15, no. 1, pp. 5–13, 2000.

[51] S. Mori, W. H. Barker, C.-Y. Chong, and K.-C. Chang, "Track association and track fusion with nondeterministic target dynamics," *IEEE Trans. on Aerosp. Electron. Systems*, vol. 38, no. 2, pp. 659–668, 2002.

[52] S. Mori and C.-Y. Chong, "Track-to-track association metric I.I.D.-non-Poisson cases," in *Proc. of the 6th International Conference of Information Fusion*, vol. 1, July 2003, pp. 553–559.

[53] L. M. Kaplan, Y. Bar-Shalom, and W. D. Blair, "Assignment costs for multiple sensor track-to-track association," *IEEE Trans. on Aerosp. Electron. Systems*, vol. 44, no. 2, pp. 655–677, 2008.

[54] S. Mori, K. Chang, and C. Chong, "Performance prediction of feature-aided track-to-track association," *IEEE Trans. on Aerosp. Electron. Systems*, vol. 50, no. 4, pp. 2593–2603, 2014.

[55] X. Tian, T. Yuan, and Y. Bar-Shalom, "Track-to-track fusion in linear and nonlinear systems," in *Advances in Estimation, Navigation, and Spacecraft Control*. Berlin, Heidelberg: Springer Berlin Heidelberg, 2015, pp. 21–41.

[56] S. Mori, K.-C. Chang, and C.-Y. Chong, "Comparison of track fusion rules and track association metrics," in *Proc. of the 15th FUSION*, July 2012, pp. 1996–2003.

[57] M. Beard, B. T. Vo, and B.-N. Vo, "OSPA$^{(2)}$: using the OSPA metric to evaluate multi-target tracking performance," in *Proc. of the 7th ICCAIS*, Oct 2017, pp. 86–91.

[58] M. Beard, B. T. Vo, and B. Vo, "Performance evaluation for large-scale multi-target tracking algorithms," in *Proc. of the 21st FUSION*, July 2018, pp. 1–5.

[59] ——, "A solution for large-scale multi-object tracking," *IEEE Trans. on Signal Process.*, vol. 68, pp. 2754–2769, 2020.

[60] D. Schuhmacher, B.-T. Vo, and B.-N. Vo, "A consistent metric for performance evaluation of multi-object filters," *IEEE Trans. on Signal Process.*, vol. 56, no. 8, pp. 3447–3457, 2008.

[61] H. W. Kuhn, "The Hungarian method for the assignment problem," *Naval research logistics quarterly*, vol. 2, no. 1-2, pp. 83–97, 1955.

[62] J. Munkres, "Algorithms for the assignment and transportation problems," *J. of the society for industrial and applied mathematics*, vol. 5, no. 1, pp. 32–38, 1957.

[63] N. Tomizawa, "On some techniques useful for solution of transportation network problems," *Networks*, vol. 1, no. 2, pp. 173–194, 1971.

[64] J. Edmonds and R. M. Karp, "Theoretical improvements in algorithmic efficiency for network flow problems," *Journal of the ACM*, vol. 19, no. 2, pp. 248–264, 1972.

[65] R. Jonker and A. Volgenant, "A shortest augmenting path algorithm for dense and sparse linear assignment problems," *Computing*, vol. 38, no. 4, pp. 325–340, 1987.

[66] B. Ristic, B.-T. Vo, B.-N. Vo, and A. Farina, "A tutorial on bernoulli filters: theory, implementation and applications," *IEEE Transactions on Signal Processing*, vol. 61, no. 13, pp. 3406–3430, 2013.

[67] Y. Bar-Shalom and L. Campo, "The effect of the common process noise on the two-sensor fused-track covariance," *IEEE Trans. on Aerosp. Electron. Systems*, vol. AES-22, no. 6, pp. 803–805, 1986.

[68] B.-N. Vo, B.-T. Vo, and H. G. Hoang, "An efficient implementation of the generalized labeled multi-Bernoullifilter," *IEEE Trans. on Signal Process.*, vol. 65, no. 8, pp. 1975–1987, 2016.

[69] L. Xiao, S. Boyd, and S. Lall, "A scheme for robust distributed sensor fusion based on average consensus," in *Proc. of th 4th IPSN.*, 2005, pp. 63–70.

[70] J. R. Hoffman and R. P. S. Mahler, "Multitarget miss distance via optimal assignment," *IEEE Trans. on Systems, Man, and Cybernetics - Part A: Systems and Humans*, vol. 34, no. 3, pp. 327–336, 2004.

[71] H. Deusch, S. Reuter, and K. Dietmayer, "The labeled multi-Bernoulli SLAM filter," *IEEE Signal Process. Lett.*, vol. 22, no. 10, pp. 1561–1565, 2015.

[72] B. Vo, B. Vo, and M. Beard, "Multi-sensor multi-object tracking with the generalized labeled multi-Bernoulli filter," *IEEE Trans. on Signal Process.*, vol. 67, no. 23, pp. 5952–5967, Dec 2019.

Hoa Van Nguyen received his Bachelor degree in electrical engineering from Portland State University, Oregon, U.S.A in 2012, and the PhD degree in computer science from The University of Adelaide, in 2020. He is currently a Post-Doctoral Research Fellow with the School of Computer Science, The University of Adelaide. His research interests include signal processing, robotics, multi-object tracking, and multi-sensor control.

Hamid Rezatofighi is a lecturer at the Faculty of Information Technology, Monash University, Australia. Before that, he was an Endeavour Research Fellow at the Stanford Vision Lab (SVL), Stanford University and a Senior Research Fellow at the Australian Institute for Machine Learning (AIML), The University of Adelaide. His main research interest focuses on computer vision and vision-based perception for robotics, including object detection, multi-object tracking, human trajectory and pose forecasting and human collective activity recognition. He has also research expertise in Bayesian filtering, estimation and learning using point process and finite set statistics.

Ba-Ngu Vo received his Bachelor degrees in Mathematics and Electrical Engineering with first class honors in 1994, and PhD in 1997. Currently he is Professor of Signals and Systems at Curtin University. Vo is a Fellow of the IEEE, and is best known as a pioneer in the stochastic geometric approach to multi-object system. His research interests are signal processing, systems theory and stochastic geometry.

Damith C. Ranasinghe received the Ph.D. degree in Electrical and Electronic Engineering from The University of Adelaide, Australia, in December 2007. In the past, he was a Visiting Scholar with the Massachusetts Institute of Technology, Cambridge, MA, USA, and a Post-Doctoral Research Fellow with the University of Cambridge, Cambridge, U.K. Currently, he is an Associate Professor at The University of Adelaide. His research interests lie broadly in the areas of autonomous systems, machine learning, and security.